Geochemical characterization of the Oman Crust-Mantle transition zone, OmanDP Holes CM1A and CM2B.

F. Kourim[1*], M. Rospabé[2], N. Dygert[3], S. Chatterjee[4], E. Takazawa[4], K-L. Wang[1, 5], M. Godard[6], M. Benoit[7], M. Giampouras[8], K. Ishii[4], D. A-H Teagle[9], M-J. Cooper[9], P. Kelemen[10]

[1] Institute of Earth Sciences, Academia Sinica, Academia Road, Nangang, Taipei 11529, Taiwan.

[2] Research Institute for Marine Geodynamics (IMG), Japan Agency for Marine-Earth Science and Technology (JAMSTEC), 2-15 Natsushima, Yokosuka, Kanagawa 237-0061, Japan.

[3] Department of Earth & Planetary Sciences, University of Tennessee, 1621 Cumberland Ave., 602 Strong Hall, Knoxville, TN 37996, U.S.A.

[4] Department of Geology, Faculty of Science, Niigata University, Niigata 950–2181, Japan

[5] Department of Earth Sciences, National Taiwan University, No. 1, Section 4, Roosevelt Rd, Da'an District, Taipei City, 10617, Taiwan

[6] Géosciences Montpellier, CNRS, Université Montpellier, Place E. Bataillon, 34095 Montpellier, France.

[7] Géosciences Environnement Toulouse (GET), Observatoire Midi-Pyrénées, Université de Toulouse, CNRS, IRD, 14 avenue E. Belin, F-31400 Toulouse, France.

[8] Instituto Andaluz de Ciencias de la Tierra (IACT), Consejo Superior de Investigaciones Científicas–Universidad de Granada, Avd. Palmeras 4, 18100 Armilla, Granada, Spain

[9] School of Ocean & Earth Science, National Oceanography Centre Southampton, University of Southampton, European Way, Southampton SO14-3ZH, UK

[10] Lamont–Doherty Earth Observatory, Columbia University, Palisades, New York, 10964, U.S.A.

[*] Corresponding author: Fatma Kourim (k.fatna@gmail.com)

Keywords: Partial melting *vs*. melt-rock reaction; Dunites and harzburgites serpentinization and carbonation; Oman ophiolite Crust-Mantle transition; Holes CM1A and CM2B; ICDP Oman Drilling Project;

Key Points:

- The transition from the oceanic crust to the mantle of Oman has been drilled in the CM Holes during Phase 2 of the ICDP Oman Drilling Project

- There is large petrological and chemical variability in the dunites and harzburgites from Holes CM1A and CM2B
- Partial melting *vs*. melt-rock reaction, and the effects of serpentinization and carbonation of dunites and harzburgites are investigated

Abstract

The transition from the gabbroic oceanic crust to the residual mantle harzburgites of the Oman ophiolite has been drilled at Holes CM1A and CM2B (Wadi Tayin massif) during Phase 2 of the International Continental Scientific Drilling Program (ICDP) Oman Drilling Project (OmanDP) (Nov. 2017-Jan. 2018). In order to unravel the formation processes of ultramafic rocks in the Wadi Tayin massif (CM) crust-mantle transition zone and deeper in the mantle sections beneath oceanic spreading centers, our study focuses on the whole rock major and trace element compositions (together with CO_2 and H_2O concentrations) of these ultramafic rocks (56 dunites and 49 harzburgites). Despite extensive serpentinization and some carbonation, most of the trace element contents (REE, HFSE, Ti, Th, U) record high temperature, magmatic process-related signatures. Two major trends are observed, with good correlations between (1) Th and U, Nb and LREE on one hand, and between (2) HREE, Ti and Hf on the other hand. We interpret the first trend as the signature of late melt/peridotite interactions as LREE are known to be mobilized by such processes ('lithospheric process'), and the second trend as the signature of the initial mantle partial melting ('asthenospheric process'), with little or no overprint from melt/rock reaction events.

Plain Language Summary

We focus on the transition from the oceanic crust to the Earth's mantle by studying Holes CM1A and CM2B, drilled in the Oman ophiolite during Phase 2 of the International Continental Scientific Drilling Program (ICDP) Oman Drilling Project (OmanDP). Despite extensive serpentinization and some carbonation, the dunites and harzburgites from the transition zone and the mantle section show a large variability in their petrological and chemical compositions. Results indicate that most of the trace element contents (REE, HFSE, Ti, Th, U) record high temperature, magmatic process-related signatures. Two major trends are observed, with good correlations between (1) Th and U, Nb and LREE on one hand, and between (2) HREE, Ti and Hf on the other hand. We interpret the first trend as the signature of late interactions between a percolating melt and the harzburgites and/or dunites, and the second trend as the signature of the initial mantle partial melting, with little or no overprint from melt/rock reaction events.

1 Introduction

Melts play a fundamental role in generating lithospheric mantle chemical and mineralogical heterogeneities, and have a large effect on mantle rheology, viscosity and seismic anisotropy (Batanova & Savelieva, 2009; Kelemen et al., 1997; Tommasi & Vauchez, 2015). Numerous studies have been dedicated to melt-rock interaction characterization in both the continental and the oceanic lithospheric mantle (e.g. Bodinier et al., 1990; Dalton et al., 2017; Dygert et al., 2016; Godard et al., 2008; Kelemen et al., 1998, 1990; Kelemen & Ghiorso, 1986; Parkinson & Pearce, 1998; Takazawa et al., 1992; Vauchez et al., 2005; Morgan et al., 2008; Navon & Stolper, 1987; Niu, 1997; Warren et al., 2009; Warren and Shimizu, 2010). Several studies demonstrated that trace element variations coupled with microstructural, mineralogical and petrological observations, and trace element numerical modeling, are a pertinent way to evaluate melt transport and constrain melt-peridotite processes (e.g. Navon & Stolper, 1987; Batanova et al., 1998; Godard et al., 1995; Kelemen et al., 1995; Kelemen & Ghiorso, 1986; Kourim et al., 2014; Oliveira et al., 2020). Despite all these studies, the nature of melt and/or fluids involved in the reactional processes in the oceanic upper mantle below spreading centers remains debated. One of the biggest challenges to understanding these processes is finding locations where samples that were affected

by either incomplete melt extraction or interaction with melt with samples that were not affected by either of these processes. Abyssal peridotites (e.g. Godard et al., 2008; Johnson et al., 1990; Niu, 1997; Parkinson & Pearce, 1998) and mantle xenoliths (e.g. Bedini & Bodinier, 1999; Dalton et al., 2017; Fitzpayne et al., 2018; Grégoire et al., 2001) are good candidates to study mantle processes in present-day oceanic and continental settings, but their sampling is sparse, lacking second-order geologic context and is limited to the uppermost oceanic and continental mantle.

Oman ophiolite has been instrumental in elucidating the accretion and evolution of oceanic lithosphere in present-day oceans and exhibits the largest ophiolitic exposures of oceanic lithosphere worldwide. The mantle section of the Oman ophiolite is mainly composed of depleted harzburgites and of some dunites, and has been the subject of many petrological, geochemical and structural studies (e.g. Boudier & Coleman, 1981; Ceuleneer et al., 1988; Dygert et al., 2017; Kelemen et al., 1995; Godard et al., 2000; Le Mée et al., 2004; Monnier et al., 2006; Nicolas et al., 2000; Takazawa et al., 2003). The general consensus stands that the dunites, as channels in the mantle section or massive at the crust-mantle transition, are residues of reaction between a melt undersaturated in silica at low pressure and mantle harzburgites; this reaction leads to the complete consumption of orthopyroxene and to the concomitant precipitation of olivine (e.g. Abily & Ceuleneer, 2013; Boudier & Nicolas, 1995; Braun et al., 2002; Godard et al., 2000; Kelemen et al., 1995, 1997; Koga et al., 2001; Quick, 1981b; Rabinowicz et al., 1987; Rospabé et al., 2017, 2018a, 2019a). However, the relationship between the harzburgites and the dunites, the nature of the reactant melt, and the chemical budgets related to the 'dunitization' process itself, are still debated. Oman ophiolite exposes large portions of the mantle and crust-mantle transition zone, suitable to understanding local to large scale studies of mantle heterogeneities and melt/peridotite reaction processes. The Oman Drilling Project (OmanDP) enabled sampling of a continuous section of the crust-mantle transition at Holes CM1A and CM2B (Wadi Tayin Massif, during Phase 2 of the ICDP OmanDP, Nov. 2017-Jan. 2018), starting from the base of the layered gabbroic crust and going through the uppermost harzburgitic mantle (Kelemen et al., 2020a, 2020b; Proceedings available at https://www.omandrilling.ac.uk/). In this paper, we characterize the major and trace element contents of the dunites and harzburgites from the Hole CM1A and CM2B drill cores to better constrain dunitization processes by first, gaining insights into Wadi Tayin mantle and crust-mantle geochemical characteristics, then, comparing these characteristics to previously studied Maqsad diapir harzburgites and mantle-crust transition zone, taking advantage of the continuous and regular, high resolution sampling performed in the Oman Drilling Project.

2 Geological setting and context of CM drill cores

2.1 Geology of the Samail ophiolite

The Samail ophiolite, located in the Sultanate of Oman and the United Arab Emirates (Fig. 1a), exposes a relatively continuous section of oceanic lithosphere, with, from top-to-depth, a 5-7 km-thick crust made of pillow basalts, a sheeted dike complex and gabbros, overlying the crust-mantle transition at the top of the upper mantle peridotites (e.g. Coleman & Hopson, 1981; Glennie et al., 1974; Searle & Malpas, 1980, Lippard et al., 1986; Nicolas et al., 1988; Nicolas, 2012 and references therein). According to the ages of pelagic sediments interbedded with basalts and of zircons in evolved gabbroic and plagiogranitic rocks, the accretion event that led to the formation of the Oman ophiolite has been estimated at around 94-97 Ma ago (Rioux et., 2012, 2013, 2016;

Tilton et al., 1981; Tippit et al., 1981; Warren et al., 2005). The tectonic setting in which the Samail ophiolite evolved is still debated. The spatial distribution along the ophiolite of the nature of the (1) mafic dikes cutting-across the mantle section, and (2) lower crustal cumulates, as well as their geochemical signature, attest that both MORB like and depleted calc-alkaline series coexisted during the igneous evolution of the ophiolite (e.g. Benoit et al., 1996; 1999; Ceuleneer et al., 1996; Clénet et al., 2010; Python & Ceuleneer, 2003; Python et al., 2008). The dikes belonging to the MORB-like volcanic units have been mapped mainly in the SE of the ophiolite and in other more restricted spots, whereas the depleted calc-alkaline series were observed at a more widespread scale (Python & Ceuleneer, 2003).

Along the Samail ophiolite, spatially constrained vertical flow structures frozen within the mantle section were interpreted as former asthenospheric diapirs distributed along the oceanic ridge (Ceuleneer, 1991; Ceuleneer et al., 1988; Jousselin et al., 1998; Nicolas et al., 1988, 2000). This mantle section is mainly composed of harzburgites (85 to 95%), relatively depleted with a typical orthopyroxene content of 15-25% and locally grading into lherzolites, and to a lesser extent of dunites (5-15%) (Boudier & Coleman, 1981; Lippard et al., 1986). The crust-mantle transition is mainly made of dunites and wehrlites and its thickness varies from a few meters to a few hundred meters (e.g. Abily & Ceuleneer, 2013; Boudier & Nicolas, 1995; Ceuleneer & Nicolas, 1985; Jousselin & Nicolas, 2000; Koga et al., 2001; Rospabé et al., 2017, 2018a).

Geochemical studies have demonstrated the overprint of partial melting and of melt/peridotite reaction processes in the mantle harzburgites' signatures (Gerbert-Gaillard, 2002; Girardeau et al., 2002; Godard et al., 2000; Hanghøj et al., 2010; Kanke & Takazawa, 2014; Khedr et al., 2014; Le Mée et al., 2004; Monnier et al., 2006; Takazawa et al., 2003). In this context, mantle dunites and dunites from the crust-mantle transition zone (CMTZ) have mostly been interpreted as replacive in origin, products of melt-harzburgite reaction leading to the complete consumption of orthopyroxene and concomitant precipitation of olivine (e.g. Abily & Ceuleneer, 2013; Boudier & Nicolas, 1995; Gerbert-Gaillard, 2002; Godard et al., 2000; Kelemen et al., 1995, 1997; Koga et al., 2001; Rabinowicz et al., 1987; Rospabé et al., 2018a). This dunitization process may have been enhanced by the involvement of a hydrous component in the reaction (Rospabé et al., 2017, 2018a, 2019a). However, a reaction origin and a cumulate origin are not mutually exclusive as it has been shown that the uppermost part (~ 20%) of the crust-mantle transition may have a composition consistent with cumulates while the main lower part (~80%) has a composition supporting the replacive origin (Abily & Ceuleneer, 2013). Furthermore, as olivine-saturated melt begins to cool conductively, hybrid processes, termed 'relative crystallization' (Collier & Kelemen 2010) produce reactive characteristics (e.g. Benn et al., 1988; Boudier and Nicolas, 1995; Koga et al., 2001; Abily and Ceuleneer, 2013; Rospabé et al., 2018a).

2.2 The crust-mantle transition at Sites CM1 and CM2

Samples studied in this paper were drilled in the Wadi Tayin massif in the SE of the ophiolite during Phase 2 of the ICDP OmanDP (Nov. 2017-Jan. 2018). According to structural and petrological maps (Gerbert-Gaillard, 2002; Python & Ceuleneer, 2003; Nicolas et al., 2000), this site is located near the border - or in an intermediate position between the border and the axis of the frozen paleo-spreading center centered on the Maqsad (Sumail massif) paleo-mantle diapir - of the MORB segment in this part of the ophiolite. The crust-mantle transition zone (CMTZ) is relatively well exposed in this area, with a clear transition from harzburgite to the north to dunites

then gabbros to the south (Fig. 1b). The two sites CM1 and CM2, separated by about 400 m, have been drilled twice: with one Hole for core recovery and a second wider Hole for geophysical logging. At these sites 400 m of core was recovered from CM1A and about 300 m of core was recovered from CM2B.

The geological map produced by the OmanDP group during the preparation of Phases 1 and 2 shows a general tilt of the units by about 30º to the south (Fig. 1c). Considering these petrological and structural configurations, Hole CM1A borehole was cored 400 m with an inclination of 60º trending to the north, in order to cut perpendicularly across the mantle-crust transition (Fig. 1d). It crosses from the gabbroic lower crust (~150 m; the Layered Gabbro "Crustal Sequence", CS), through the dunite-rich crust-mantle transition zone (~150 m CMTZ) that includes the Dunite (DS) and Dunite with Gabbro Sequences (DGS), to the residual upper mantle harzburgites (~100 m, Mantle Sequence, MS). At Site CM2, the fully cored borehole CM2B is vertical, parallel to the wider rotary borehole for geophysical logging (Hole CM2A). Hole CM2B starts within the crust-mantle transition zone (~110 m) and extends deeper in the underlying residual mantle peridotites than Hole CM1A (~180 m) (Fig. 1d). The main rock types sampled in Holes CM1A and CM2B are olivine-gabbro, gabbro, dunite, harzburgite and wehrlite, associated with minor gabbronorite, troctolite, websterite, anorthosite, and chromitite layers (Fig. 1d). The crust-mantle transition zone sampled in Hole CM1A and CM2B has been divided into two parts according to the rock types present: the upper half is mainly made of dunites containing rare melt migration features (DS for Dunite Sequence); in the lower half, the dunites alternate with thin bands containing a higher proportion of interstitial plagioclase (+/- clinopyroxene), which has been called the Dunite with Gabbro Sequence (DGS). In the present article we focus on the geochemical compositions of dunites from the crust sequence (CS), crust-mantle transition zone (CMTZ) and mantle sequence (MS) and of mantle harzburgites.

3 Results

The sample selection strategy and the analytical methods are detailed in Supporting Information (see also Kelemen et al., 2020a, 2020b, 2020c). In summary, one sample was taken every 10 m along Holes CM1A and CM2B to cover the entire crust-mantle transition and mantle sections. Additional samples were collected to better characterize some specific levels (e.g. to document local, minor lithologies). The samples were analyzed for their major (as well as volatile) and trace element compositions. Sample lithology, macroscopic and microscopic observations and mineral modes calculated from major elements are reported in supplementary data table 1. Whole rock major and volatile element compositions are reported in supplementary data table 2. Whole rock trace element compositions are reported in supplementary data table 3.

3.1. Sample description

The studied samples represent the ultramafic lithologies (harzburgites and dunites) of the mantle section (46 harzburgites and 12 dunites), the crust-mantle transition zone (45 dunites) and the crustal Layered Gabbro Sequence (2 dunites) drilled at Holes CM1A (46 samples) and CM2B (59 samples). Lithological classifications were made based on macroscopic and microscopic observations, and mineral modes calculated from XRF measurements (supplementary data table 1). Four rock groups have been defined, harzburgites (36), carbonate-bearing harzburgites (8), pure dunites (31) and impregnated dunites (29) (Fig. 1e, Fig. SD-1, supplementary data table 1).

The harzburgites and carbonate-bearing harzburgites contain olivine (ol), orthopyroxene (opx) and minor spinel (sp) as primary minerals (Fig. 2 e, f, g, h, i, j, k and l, Fig. SD-1, supplementary data table 1), displaying a porphyroclastic texture. Olivine abundance (primary mode) ranges from 72% to 93% in the harzburgites and from 64% to 75% in carbonate-bearing harzburgites. The olivine typically show subhedral shape and equant habits. Orthopyroxene abundance ranges from 10 to 28 % with mostly subhedral shapes; some orthopyroxene show sigmoidal crystal-plastic deformation features (Fig. 2i and j). Grains of spinel are present in all samples (up to 1-3%). Compared to the dunites, the harzburgites are less altered, the alteration becoming complete only in highly veined zones and at the bottom of both Holes where carbonate (carb)/serpentine (serp) associations occur (Fig. 2k and l). The most abundant minerals in the harzburgite background alteration are serpentine and magnetite (mag). The carbonate alteration occurs at the bottom of both Holes starting at 388.3m depth in CM1A and at 279.5m depth in CM2B. Harzburgite sample CM2B 129Z1 5-10 cm (depth 299.7 m) is the most carbonate vein-rich harzburgite. Secondary amphibole (amph), chlorite (chl) and hydrogrossular are also present as trace alteration minerals (abundance < 3%, supplementary data table 1). No patch or deformation features specifically related to the alteration were observed.

The pure dunites are primarily composed of ol >97% and generally contain <1 % sp (Fig. 2a, b, c and d, supplementary data table1). Mineral modes calculated using bulk rock data (Fig. SD-1, supplementary data table1) indicate that many dunites have >10% *normative* pyroxene. The macroscopic and microscopic descriptions indicate that some dunites contain plagioclase (pl) and/or pyroxenes. We refer to this group of dunites as 'impregnated dunites' in contrast to the pure dunites containing only ol and sp. The ol in almost all samples has been completely replaced by serp (Fig. 2a, b, c and d). In many dunites and in impregnated dunites, no relics of porphyroclastic opx are present, indicating no textural relics of a porphyroclastic texture. The pure and impregnated dunites' primary texture was a fine- to medium-grained granular microstructure, characterized by euhedral ol forming a mosaic of equigranular grain size distribution as preserved by the equant contacts between serp mesh cores (Fig. 2a, b, c and d). Alteration minerals mainly consist of serp and mag (Fig. 2a, b, c and d). In addition, brucite (brc) after ol was detected by X-Ray Diffraction (XRD, performed during the ChikyuOman 2018 Leg 3) in some serpentinized dunites from the crust-mantle transition zone and in dunites from the mantle sequence (absent in harzburgites). Where relics of ol are present, in rare cases, they are surrounded by serp and mag. If ol is completely serpentinized, the mesh cores are mainly composed of serp with minor mag and accessory grains of sulfides (These sulfides are equant and anhedral, they have grain sizes of 0.1–1 mm, modes of 0.5%, and are very rich in Ni, Kelemen et al., 2020a, 2020b - see also Lorand, 1988 for an article dedicated the the study of sulfides in Oman peridotites). Serpentine and more abundant magnetite at mesh rims trace former ol grain and sub-grain boundaries (Fig. 2a, b, c and d).

3.2. Loss on ignition, CO_2 and H_2O contents

Samples from Holes CM1A and CM2B display high loss on ignition (LOI) values. The LOI varies from 8.29 to 14.92 wt.% in the harzburgites, from 9.02 to 23 wt.% in the carbonate-bearing harzburgites, from 10.14 to 15.31 in the pure dunites and from 6.14 to 15.53 wt.% in the impregnated dunites (Fig. 3 and supplementary table 2). The averaged H_2O concentration is 12.0 ± 1.7 wt.% in harzburgites, 11.0 ± 5.5 wt.% in carbonate-bearing harzburgites, 14.3 ± 1.2 wt.% in

253 dunites and 13.7 ± 1.6 wt.% in impregnated dunites. The LOI values correlate with measured water
254 concentration (H_2O), which slightly decreases downhole (Fig. 3). The concentrations of CO_2
255 measured in harzburgites, carbonate-bearing harzburgites excluding the carbonate vein-rich
256 harzburgite CM2B 129Z1 5-10 cm (depth 299.7 m, CO_2 = 19.54 wt.%), pure dunites and
257 impregnated dunites vary from 0.12 to 0.31 wt.%, from 0.36 to 1.30 wt.%, from 0.13 to 0.34 wt.%
258 and from 0.03 to 0.41 wt.% respectively. The averaged $CaCO_3$ concentration excluding the
259 carbonate-rich harzburgite mentioned previously (22.77 wt.%), is 0.40 wt.% in harzburgites, 1.57
260 wt.% in carbonate-bearing harzburgites, 0.51 wt.% in pure dunites and 0.46 wt.% in impregnated
261 dunites. The downhole profile of $CaCO_3$ shows an increase in concentration in the deepest part of
262 Holes CM1A and CM2B, with recovered harzburgites having higher CO_2 concentrations, LOI and
263 H_2O contents, consistent with the particularly high alteration degree and high carbonate content in
264 these samples (serp, brc, carb, see Fig. 3 XRD).

265 **3.3. Whole rock major element compositions**

266 Major element analyses were performed on 36 harzburgites, 8 carbonate-bearing harzburgites, 31
267 pure dunites, and 29 impregnated dunites sampled along Holes CM1A and CM2B.

268 *The mantle section sequence (MS)*

269 Harzburgite is the most abundant lithology in the MS (36 harzburgites analysed) followed by
270 impregnated dunite (9 impregnated dunites analysed) and pure dunite (4 pure dunites analysed).
271 Mg# (Mg# = 100 × molar Mg/(Mg+Fe_{total})) in mantle harzburgites is between 90.7 and 92.4. CaO,
272 Al_2O_3, and TiO_2 contents range from 0.19 to 2.07 wt.%, 0.53 to 0.91 wt.%, and 0.02 to 0.04 wt.%,
273 respectively (Fig. 4). Harzburgite with dunite patches contains lower CaO concentrations than the
274 average value (0.30 to 0.81 wt.%). Carbonate-bearing harzburgites are characterized by similar
275 Mg#, Al_2O_3, and TiO_2 contents (90.6, 0.70 wt.% and 0.03 wt.% on average respectively), and very
276 high CaO concentrations ranging from 0.68 to 5.42 wt.% compared to carbonate-free harzburgites.
277 Dunites from the MS have high Mg#, on average 90.2 for pure dunites and 91.1 for impregnated
278 dunites (Fig. 4). The pure dunites have CaO, Al_2O_3 and TiO_2 contents from 0.30 to 0.94 wt.%,
279 0.32 to 0.72 wt.%, and 0.02 to 0.05 wt.% respectively, where the impregnated dunites have CaO
280 contents ranging from 0.14 to 1.59 wt.%, Al_2O_3 from 0.21 to 0.95 wt.% and TiO_2 from 0.02 to
281 0.04 wt.% (Fig. 4). Along the MS, TiO_2 and Al_2O_3 contents do not show any systematic variation
282 with depth. On the other hand, the CaO content shows some variations downhole. The vertical
283 evolution of the CaO content in harzburgites from Hole CM1A is different from other elements;
284 successive trends of increasing and decreasing CaO with depth form a well-defined zigzag pattern
285 In detail, it increases from 0.97 to 2.1 wt. % between 311 and 340 m and from 0.54 to 1.8 wt.%
286 between 360 and 388 m, and decreases from 2.1 to 0.54 wt. % between 340 and 360 m then from
287 1.8 to 0.8 wt.% at most from 388 to around 400 m. CaO contents in dunites and nearby harzburgites
288 are correlated. Downhole intervals with the highest CaO contents are characterized by high
289 carbonate vein concentrations (Fig. 3 XRD, and Fig. 4).

290 *The crust-mantle transition zone sequence (CMTZ)*

291 The CMTZ is composed mainly of pure and impregnated dunites (Fig. 1d). 27 pure dunites and 18
292 impregnated dunites from Holes CM1A and CM2B CMTZ were analyzed. Both pure and
293 impregnated dunites from the CMTZ display slightly lower Mg# (89.9 on average, Fig. 4) and

CaO concentrations (pure dunites = 0.16 wt.%, and impregnated dunites = 0.28 wt.% on average, Fig. 4) compared to the dunites from the MS. Some dunites from CM1A DGS (between 252.96 and 271.42 m) display lower Mg# (Mg# = 86.8-88.0) that seems mostly controlled by the increase in the FeO content. The TiO_2 contents in pure and impregnated dunites from the CMTZ (0.04 wt.% on average) are slightly higher than the TiO_2 contents in the MS dunites (0.03 wt.% on average). Al_2O_3 concentrations are lower in CMTZ pure dunites (0.42 wt.% on average) and higher in impregnated dunites (1.12 wt.% on average) compared to pure (0.53 wt.% on average) and impregnated (0.51 wt.% on average) dunites respectively from the MS. A similar zigzag pattern to the one observed in CaO along the MS is irregularly observed in CMTZ dunites (i.e. in CM1A, decreasing from 0.17 to 0.12 wt. % between 170 and 245 m and, increasing from 0.08 to 0.52 wt. % between 253 and 310 m, Fig. 4). This CaO zigzag variation in CM1A CMTZ dunites is associated with Mg# zigzag variation (decreasing from 91 to 89 wt. % between 170 and 245 m and, increasing from 87 to 91 wt. % between 253 and 310 m, Fig. 4). The dunites' CaO varies over ~ 20 m at the base of the CMTZ following the mantle harzburgites zigzag variation, whereas the Mg# varies over ~ 60 m, along with the FeO variations.

The crustal sequence (CS)

The two analyzed dunites from the Layered Gabbro Sequence (LGS) (C5707A-51Z-1 W, 31.0-39.0 cm, 125.60 m in depth, and C5707A-58Z-2 W, 1.0-6.0 cm, 143.93 m in depth) are impregnated (Fig. 4), they have relatively low Mg# (85.6 and 85.5 respectively), compared to dunites in the other sequences. This tendency is similar to the dunites from CM1A DGS. CaO (0.04 wt.% and 0.19 wt.% respectively), Al_2O_3 (0.15 wt.% and 0.93 wt.% respectively) and TiO_2 (0.03 wt.%) contents are similar to the impregnated dunites values from the MS and the CMTZ (Fig. 4).

CM Holes harzburgites, carbonate-bearing harzburgites, pure dunites and impregnated dunites (except CM1A LGS impregnated dunites) show comparable major element compositions to previously reported harzburgites, dunites and impregnated dunites from the Oman ophiolite mantle and crust-mantle transition zones (Fig. 5). Most of the pure and impregnated dunites from MS, and CMTZ plot above the terrestrial array (Earth differentiation trend, Jagoutz et al., 1979) in the MgO/SiO_2 vs. Al_2O_3/SiO_2 diagram, similar to previously studied dunites and impregnated dunites from the mantle section of Wadi Tayin massif (Godard et al., 2000; Hanghøj et al., 2010) and the CMTZ at the top of Maqsad diapir (Rospabé et al., 2018a, 2019a) (Fig. 5a). Whereas the harzburgites, carbonate-bearing harzburgites and some pure and impregnated dunites plot below. The MgO-FeO variations in most of the CM dunites mimic the stoichiometric variation of the ol Mg-Fe composition, similar to other pure/slightly impregnated dunites elsewhere, while only a few CM samples fall in the domain of the more highly impregnated dunites. Lower CaO and wider range of Al_2O_3 values characterize all the dunites compared to the harzburgites (Fig. 5). Similar to other previously studied Wadi Tayin massif and Maqsad diapir harzburgites (Godard et al., 2000; Hanghøj et al., 2010; Monnier et al., 2006) and most refractory abyssal peridotites (Godard et al., 2008; Niu, 1997; Warren et al., 2009), CM harzburgites plot near the most depleted end of the mantle fractionation array (Fig. 5a). They display similar low Al_2O_3/SiO_2 ratios in comparison to other harzburgites from Wadi Tayin and Maqsad harzburgites (0.01-0.02, 0.01-0.04 and 0.01-0.08 respectively), and a high MgO/SiO_2 ratios typical of refractory peridotites (0.98-1.10, 0.95-1.10 and 0.96-1.15 respectively). Oman harzburgites are characterized by narrow FeO and MgO contents compared to the pure and impregnated dunites (Fig. 5b), with slightly higher Mg# in CM

harzburgites (90.7-92.4) compared to Wadi Tayin and Maqsad harzburgites (89.6-91.5 and 88.4-91.1 respectively). Generally, Al_2O_3 and CaO show broad positive correlation in harzburgites from Wadi Tayin massif and Maqsad diapir (Fig. 5c), Godard et al, (2000) demonstrating that the observed Al_2O_3/CaO ratio variability displayed by Wadi Tayin and Maqsad harzburgites decreases with increasing cpx content in the main harzburgites sequence to lower values in the *cpx*-harzburgites at the base of the mantle section. Al_2O_3/CaO ratio variability is also observed along cores CM1A and CM2B, however CaO variability at the bottom of CM Holes is related to CO_2-bearing fluids interactions with CM harzburgites (see section 4.1.).

3.4.Whole rock trace element contents

Chondrite-normalized Rare Earth Element (REE) and primitive mantle-normalized trace element variations and patterns are shown in Figures 6 and 7 respectively. Similar to other refractory peridotites from the Oman ophiolite mantle section and crust-mantle transition, the studied harzburgites, carbonate-bearing harzburgites, pure dunite and impregnated dunite whole rock concentrations are lower than chondritic (CN) and primitive mantle (PM) values (Figs. 6 and 7). Their REEs are characterized by three types of chondrite-normalized patterns: linear or flat linear, U- or V-shaped, and concave-upward patterns. CM Holes show vertical trends, continuous over tens of meters, in their REE content. These are characterized by ~ 50 m-thick alternations between increasing and decreasing concentrations ('zigzag' patterns) (e.g. La, Yb, LREE patterns; Fig. 6). These trends along CM Holes are observed in both dunites and harzburgites, independent of the lithology, and the changes from one trend to another are commonly correlated with the presence of faults described by the structural team during the ChikyuOman2018 Leg 3 (Kelemen et al., 2020a, 2020b).

The mantle section sequence

The mantle harzburgites show two types of chondrite-normalized REE patterns: (1) 19 harzburgites display linear REE patterns characterized by a progressive depletion from heavy REE (HREE) (Gd_{CN}/Yb_{CN}= 0.25 ± 0.21, Yb_{CN} = 0.22 ± 0.11) to middle REE (MREE: Sm, Eu and Gd) (Sm_{CN} = 0.06 ± 0.05 and Gd_{CN} = 0.06 ± 0.05) and light (LREE) (La_{CN}/Sm_{CN} = 0.98 ± 0.74, La_{CN} = 0.06 ± 0.05). 6 samples show a positive Eu anomaly ($(Eu/Eu^*)_{CN}$ = 2.36 ± 0.66, with $(Eu/Eu^*)_{CN}$ = $Eu_{CN}/\sqrt{(Sm_{CN} \times Gd_{CN})}$). In detail, 12 harzburgites display linear LREE-depleted patterns (3 from CM1A and 9 from CM2B) characterized by a progressive depletion from HREE to LREE, and 7 harzburgites (5 from CM1A and 2 from CM2B) display flat linear REE patterns characterized by slightly lower LREE concentrations compared to HREE concentrations. (2) 15 harzburgites (4 from CM1A and 11 from CM2B) display U- or V-shaped REE patterns reflecting significant MREE depletion relative to LREE (La_{CN}/Sm_{CN} = 3.21 ± 1.18) and HREE (Gd_{CN}/Yb_{CN} = 0.07 ± 0.06). 7 samples show a positive Eu anomaly ($(Eu/Eu^*)_{CN}$ = 3.36 ± 1.69).

The mantle pure dunites and impregnated dunites show two types of chondrite-normalized REE patterns: linear REE patterns (3 pure dunites from CM2B and 6 impregnated dunites (3 from CM1A and 3 from CM2B)) and U- or V-shaped REE patterns (5 pure dunites and 1 impregnated dunites from CM2B). In detail the linear REE pattern are subdivided to: (1) flat linear REE patterns displayed by the three CM1A impregnated dunites, they are characterized by roughly similar

LREE (La_{CN} = 0.14 ± 0.07), MREE (Sm_{CN} = 0.10 ± 0.05), and HREE (Yb_{CN} = 0.18 ± 0.05) concentrations, together with a positive Eu anomaly ($(Eu/Eu^*)_{CN}$ = 2.06 ± 0.65). (2) LREE-depleted linear REE patterns displayed by 3 pure dunites and 3 impregnated dunites from CM2B show a progressive depletion from HREE (Gd_{CN}/Yb_{CN}= 0.25 ± 0.16 and 0.18 ± 0.04, Yb_{CN} = 0.22 ± 0.05 and 0.28 ± 0.07 respectively) to MREE (Sm_{CN} = 0.04 ± 0.03 and 0.04 ± 0.02, Gd_{CN} = 0.06 ± 0.04 and 0.05 ± 0.02 respectively) to LREE (La_{CN}/Sm_{CN} = 0.71 ± 0.28 and 0.37 ± 0.23, La_{CN} = 0.03 ± 0.02 and 0.02 ± 0.01 respectively), 1 sample shows a positive Eu anomaly $(Eu/Eu^*)_{CN}$ = 1.60). The U- or V-shaped REE patterns (5 pure dunites and 1 impregnated dunites from CM2B) are characterized by significant MREE depletion relative to LREE (La_{CN}/Sm_{CN} = 2.66 ± 1.76) and HREE (Gd_{CN}/Yb_{CN} = 0.08 ± 0.12), 2 pure dunites display a positive Eu anomaly ($(Eu/Eu^*)_{CN}$ = 2.91 and 2.54).

The crustal-mantle transition zone sequence (CMTZ)

The pure dunites from the CMTZ show two types of chondrite-normalized REE patterns: (1) U-shaped REE pattern displayed by 11 pure dunites (6 from CM1A and 5 from CM2B), with MREE depletion relative to LREE (La_{CN}/Sm_{CN} < 3.34) and HREE (0.07 < Gd_{CN}/Yb_{CN} < 0.27). Some samples also have positive Eu anomalies (4 samples from CM1A and 3 samples from CM2B, $(Eu/Eu^*)_{CN}$ = 3.62 ± 2.49). (2) Linear LREE-depleted or slightly concave-upward REE patterns displayed by 10 pure dunites from Hole CM1A (La_{CN}/Yb_{CN} = 0.07 ± 0.05) with similar HREE concentrations (Yb_{CN} = 0.13 ± 0.02) and lower LREE and MREE variation compared to HREE (La_{CN} = 0.01 ± 0.01; Gd_{CN} = 0.02 ± 0.01). Most samples display a positive Eu anomaly (6 samples, $(Eu/Eu^*)_{CN}$ = 4.43 ± 2.44).

The CMTZ impregnated dunites display three types of chondrite-normalized REE patterns: (1) The linear REE patterns displayed by 5 impregnated dunites (2 from CM1A and 3 from CM2B) are characterized by a progressive depletion from HREE (Gd_{CN}/Yb_{CN}= 0.38 ± 0.20, Yb_{CN} = 0.23 ± 0.09) to MREE (Sm_{CN} = 0.07 ± 0.06 and Gd_{CN} = 0.10 ± 0.09) to LREE (La_{CN}/Sm_{CN} = 0.77 ± 0.19, La_{CN} = 0.05 ± 0.06), 2 samples show a positive and negative Eu anomaly ($(Eu/Eu^*)_{CN}$ = 2.23 and 0.45 respectively). (2) 3 samples from CM2B display U-shaped REE pattern, with MREE depletion relative to LREE (La_{CN}/Sm_{CN} < 3.93) and HREE (0.09 < Gd_{CN}/Yb_{CN} < 0.25). (3) One sample from CM1A and three samples from CM2B display concave-upward patterns characterized by a nearly flat slope of the HREE segment (Gd_{CN}/Yb_{CN} = 0.86 ± 0.39) followed by a progressive depletion from MREE to LREE (La_{CN}/Sm_{CN} = 0.13 ± 0.07). One CM1A impregnated dunite shows a negative Eu anomaly ($(Eu/Eu^*)_{CN}$ = 0.42).

The crustal sequence (CS)

The two impregnated dunites from the Hole CM1A CS (C5707A-51Z-1 W, 31-39.0 cm, 125.60 m depth, and C5707A-58Z-2 W, 1.0-6.0 cm, 143.94 m depth) display relatively linear (REE) patterns characterized by a steady decrease of REE abundances HREE to LREE, as well as by a clear positive Eu anomaly ($(Eu/Eu^*)_{CN}$ = 3.8-5.0).

The PM-normalized multi-element patterns of most harzburgites and carbonate-bearing harzburgites exhibit strong to moderate enrichments in LILE, Th, U, Nb and Ta relative to LREE (e.g. averaged Rb_{PMN}/La_{PMN} = 12.95 and 18.24; U_{PMN}/La_{PMN} = 4.64 and 4.45; Nb_{PMN}/La_{PMN} = 2.02 and 4.30 respectively). The carbonate-bearing harzburgites display stronger Pb, Sr and Ti positive

anomalies (averaged Pb_{PMN}/Ce_{PMN} = 145.23; Sr_{PMN}/Nd_{PMN} = 373.50; Ti_{PMN}/Gd_{PMN} = 11.09) compared to the harzburgite (averaged Pb_{PMN}/Ce_{PMN} = 25.83; Sr_{PMN}/Nd_{PMN} = 30.21, Ti_{PMN}/Gd_{PMN} = 3.52). Most pure dunites show similar enrichments exhibited by the harzburgites and carbonate-bearing harzburgites in LILE, Th, U, Nb and Ta relative to LREE (e.g. averaged Rb_{PMN}/La_{PMN} = 20.0; U_{PMN}/La_{PMN} = 5.12; Nb_{PMN}/La_{PMN} = 4.10), but with smaller Pb and Sr positive anomalies (averaged Pb_{PMN}/Ce_{PMN} = 19.68; Sr_{PMN}/Nd_{PMN} = 29.05). The pure dunites display stronger Ti positive anomalies compared to the harzburgites and smaller compared to the carbonate-bearing harzburgites (Ti_{PMN}/Gd_{PMN} = 8.98). The impregnated dunites exhibit moderate LILE, Th, U, Nb and Ta enrichments relative to LREE (e.g. averaged Rb_{PMN}/La_{PMN} = 3.94; U_{PMN}/La_{PMN} = 3.12; Nb_{PMN}/La_{PMN} = 1.05), and the smallest Pb, Sr and Ti positive anomalies compared to all groups of rocks (averaged Pb_{PMN}/Ce_{PMN} = 9.99; Sr_{PMN}/Nd_{PMN} = 14.03; Ti_{PMN}/Gd_{PMN} = 1.62).

4 Discussion

Most studies of the ultramafic rocks from the Oman ophiolite consider the dunites to be channels in the mantle or massive at the crust-mantle transition, and replacive in origin. In this model, the dunites represent residues of reaction between a melt undersaturated in silica at low pressure and the host mantle harzburgites during a melt percolation event that led to the complete consumption of orthopyroxene and to the concomitant precipitation of olivine (e.g. Abily & Ceuleneer, 2013; Boudier & Nicolas, 1995; Braun et al., 2002; Godard et al., 2000; Kelemen et al., 1995, 1997; Koga et al., 2001; Rabinowicz et al., 1987; Rospabé et al., 2017, 2018a, 2019a). The hypothesis of the replacive origin of the dunites, also proposed for other ophiolitic sections and for dunites associated with abyssal peridotites (e.g. Dick & Natland, 1996; Kelemen et al., 1990; Godard et al., 2008; Quick, 1981a, 1981b), contrasts with an older cumulative model, in which ol crystallization and accumulation created the lowermost part of the oceanic crust (e.g. Elthon, 1979; O'Hara, 1965; Smewing, 1981). Alternatively, it has been proposed that the crust-mantle transition of the Oman ophiolite may be of double origin, with the lower 80% as replacive and the upper 20% as cumulates (Abily & Ceuleneer, 2013). In the case of the OmanDP CM cores, the alternations between dunites and mantle harzburgites at the top of the mantle sequence is consistent with a melt/rock reaction origin, a feature observed at crust-mantle transitions of many massifs along the Oman ophiolite (e.g. Boudier & Nicolas, 1995) and that cannot be accounted for by a simple fractional crystallization process.

Structural and petrological mappings of the Oman ophiolite have revealed contrasting domains along the ophiolite. Especially, the spatially varying nature and composition of the dikes cross-cutting the mantle section reflect formation involving a MORB-like melt mainly in the south-eastern Nakhl, Samail and Wadi Tayin massifs (troctolite and ol-gabbro dikes), contrasting with a more widespread depleted, calc-alkaline magma composition elsewhere (mostly gabbronorite and pyroxenite dikes) (Python & Ceuleneer, 2003; Python et al., 2008). The MOR-like area characterizes a NW-SE oriented paleo-spreading segment that seems to have developed within older, already accreted lithosphere of depleted calc-alkaline affinity (Ceuleneer et al., 1988; 1996; Gerbert-Gaillard, 2002; Godard et al., 2000; Nicolas et al., 2000; Python & Ceuleneer, 2003). This MORB segment is hypothesized to have been centered on, and fed with melts by, the fossil mantle diapir of the Maqsad area in the Samail massif (Rabinowicz et al., 1987; Ceuleneer et al., 1988; Jousselin et al., 1998). According to the published structural and petrological maps, the drilling site is located within the area where melts were MORB-like, near the NE limit of the paleo spreading segment. This delimitation has been defined as the Makhibiyah shear zone in the Wadi

Tayin massif, making the contact with the older lithosphere (Nicolas & Boudier, 2008). Accordingly, it is reasonable to consider that a MORB-like melt played an important role in the formation of the CM dunites and harzburgites.

4.1 Effects of serpentinization and carbonation on the composition of dunites and harzburgites

In some cases, alteration, especially serpentinization of ultramafic rocks (sometimes associated with mineralization related to hydrothermal activity), may significantly modify bulk-rock chemical composition (e.g. Beinlich et al., 2020; de Obeso & Kelemen, 2018; Gruau et al., 1998; Hodel et al., 2018; Malvoisin, 2015; Paulick et al., 2006; Snow & Dick, 1995). As described above, the dunites and harzburgites from the crust-mantle transition and mantle section of Holes CM1A and CM2B are extensively serpentinized (Fig. 2), up to 100% in many samples. In addition, strong carbonate-veining affected parts of the cores, especially at the base of Hole CM2B where it is intensely faulted (carbonate-bearing harzburgites, Fig. 3, CO_2 and $CaCO_3$ logs). To decipher the effects of such significant fluid/rock interactions on the composition of OmanDP CM samples is critical (especially on the trace elements). It particularly concerns the dunites, because of their more altered character (perhaps related to higher ol mode), and because their trace element budget was more significantly controlled by primary ol and trace phases such as pyroxenes before alteration (unlike the harzburgites that contain abundant residual pyroxenes).

The LOI content is generally higher in carbonate-bearing harzburgite (averaged LOI = 13.04 ± 9.57 wt.%), pure dunites (averaged LOI = 13.92 ± 1.21 wt.%) and impregnated dunites (averaged LOI = 13.33 ± 2.02 wt.%) than in harzburgites (averaged LOI = 11.91 ± 1.53 wt.%). Serpentinization of many of the studied samples appears to have led to enrichment in SiO_2 as already observed in abyssal peridotites affected by a Si addition, and/or magnesium loss (e.g. de Obeso & Kelemen, 2018; Paulick et al., 2006; Snow & Dick, 1995). This open system behavior is confirmed by the plot of some dunites (3 from CM2B) and impregnated dunites (4 from CM1A and 4 from CM2B) below the mantle fractionation array at the same field as the harzburgites and the carbonate-bearing harzburgites (Fig. 5a), suggesting MgO loss and/or SiO_2 enrichment as reported in pervasively serpentinized abyssal peridotites or talc-bearing serpentinites (de Obeso & Kelemen, 2018; Snow & Dick, 1995; Paulick et al., 2006). This may be the reason why there are elevated normative pyroxene modes in samples that were classified as dunites based on macroscopic (hand specimen) and microscopic (thin sections) observations (Fig. SD-1, supplementary data table 1). Some of these dunites have no pyroxenes or pyroxene pseudomorphs in thin section. This is supported by XRD analyses performed during ChikyuOman 2018 Phase 2 Leg 3 which revealed the widespread occurrence of brucite associated with other alteration minerals (Kelemen et al., 2020a, 2020b). It also appears clear that the higher $CaCO_3$ (averaged $CaCO_3$ = 3.93 ± 10.85 wt.% compared to 0.40 ± 0.54 wt.% in harzburgites) together with higher CO_2 contents (averaged CO_2 = 2.82 ± 9.501 wt.% compared to 0.20 ± 0.25 wt.% in harzburgites) in the carbonate-bearing harzburgites at the base of CM1A and CM2B (4 from CM1A and 4 from CM2B) are related to carbonate-veins. However, the covariation of Ni and Co contents with the

XMg suggests that the possible precipitation of sulfides (Kelemen et al., 2020a, 2020b) related to these strong water/rock interactions did not erase the primary compositions in these elements.

The plots of the concentration of several trace elements as a function of the LOI (Fig. 8a-c) and of the CO_2 and $CaCO_3$ contents show no clear correlation. On the contrary, some reasonably good covariations are observed between Th and U, Nb and especially La on one hand (Fig. 8 h-j), and Yb, Ti and Hf on the other hand (Fig. 8 n-o); the Zr content is partially correlated with both Th and Yb (Fig. 8 f, k). Since Th and Ti are generally considered immobile during alteration processes (e.g. Kogiso et al., 1997; Niu, 2004; Paulick et al., 2006), these trends probably reflect one or more overlapping geochemical signatures acquired during high temperature, magmatic processes rather than during a later serpentinization event. The large ion lithophile elements as well as Li and Pb do not correlate with the LOI nor with other elements (Fig. 8 b, c, g, l, m), and their compositions may result from the overprint of several processes having operated over a large range of temperatures and conditions, from igneous to alteration events. Accordingly, only the concentrations in REE, HFSE and Th-U, will be used to discuss the igneous processes that led to the formation of the dunites from the crust-mantle transition zone and mantle sequence sampled by the CM Holes.

4.2. Partial melting *vs.* melt-rock reaction in the Oman ophiolite mantle section

The mantle section of CM Holes (Wadi Tayin massif) is composed of refractory harzburgites with relatively homogeneous modal and major element compositions (excluding some major elements e.g. CaO and Na_2O, Figs. 4 and 5) and more variable trace element contents (Figs. 6, 7a and 7b). Significant geochemical variability of the mantle peridotites has also been observed all along the Oman ophiolite. In some cases, previous geochemical studies inferred the overprint of partial melting and melt/peridotite reaction processes in the mantle harzburgite signatures (e.g. Gerbert-Gaillard, 2002; Girardeau et al., 2002; Godard et al., 2000; Hanghøj et al., 2010; Kanke & Takazawa, 2014; Khedr et al., 2014; Le Mée et al., 2004; Monnier et al., 2006; Takazawa et al., 2003). Two different geochemical trends are combined in the trace element contents of all samples studied here. On one hand, Yb shows a good correlation with Ti and some HFSE (Fig.8o). Heavy REE have been demonstrated to be less impacted than MREE and especially LREE during melt-peridotite reactions such as melt/rock re-equilibration during melt migration or in response to conversion of harzburgite to dunite (e.g. Godard et al., 1995; Kelemen et al., 1990; Navon & Stolper, 1987; Prinzhofer & Allègre, 1985; Spiegelman & Kelemen, 2003; Vernières et al., 1997; Rospabé et al., 2018a). Therefore, these correlations may have been formed during partial melting, with little or no overprint by subsequent melt-peridotite interactions at shallow depth. On the other hand, we observe a good correlation between Th, U and La, and partially with the HFSE (e.g. Nb, Fig. 8h-j), that does not correlate with Yb or Ti concentrations. As the U-/V-shape of the REE patterns, resulting from the selective enrichment in LREE relative to MREE and HREE in peridotites, may be attributed to chromatographic fractionation associated with interstitial melt percolation and/or to the transformation of harzburgite into dunite (e.g. Godard et al., 1995; Navon & Stolper, 1987; Prinzhofer & Allègre, 1985; Vernières et al., 1997; Rospabé et al., 2018a), we interpret this second geochemical signature as the overprint of melt-peridotite reaction processes.

4.2.1. Geochemical logs

Vertical chemical trends are observed along CM Holes, especially in REE (e.g. La, Yb; Fig. 6), and in some major elements (e.g. FeO, MgO, CaO, Na_2O; Fig. 4). These chemical trends are

continuous over tens of meters, and alternate between increasing and decreasing ('zigzag' patterns) with a characteristic thickness of ~ 50 m. Abrupt changes in these trends, particularly in Yb, LREE and HREE concentrations, are mostly associated with the presence of faults (Fig. 6). The trends observed in CM1A and CM2B dunites and harzburgites do not show any significant correlation as a function of LOI, CO_2, or $CaCO_3$ contents (Figs. 3 and 8). This, together with the continuity of each individual trend, suggests that the trends were imprinted at high temperature and are not related to post-magmatic, low temperature events. Furthermore, the trends are observed in both dunites and harzburgites in the mantle section, independent of dunite and harzburgite alternations. Similar trend changes attributed to the focus of the percolation/migration of melts or HT fluids along faults have been observed for the Maqsad CMTZ dunites, with the same characteristic thickness of about 50 m (Rospabé et al. 2019a, 2020). Our results seem to confirm the significant impact of deep-seated syn-magmatic faults on the development of the crust-mantle transition at the expense of the shallower mantle and the recorded whole rock chemical signatures, in addition to their impact on the formation of the lower oceanic crust (Abily et al., 2011, 2021; see also Sauter et al., 2021). Such structural characters must have developed early and are not just restricted to the Maqsad area (e.g. Rospabé (2018) and Abily et al. (2021) for other Oman areas and Sauter et al. (2021) for present-day oceans).

4.2.2. The origin of the harzburgite REE pattern shapes and cryptic and modal mantle refertilization in Oman ophiolite

CM mantle harzburgites display two types of chondrite-normalized REE patterns: (1) linear to flat linear REE patterns characterized by a progressive depletion from HREE to MREE to LREE, some samples show similar LREE and HREE concentrations and slightly lower LREE and MREE variation compared to HREE; (2) U- or V-shaped REE patterns reflecting significant MREE depletion relative to LREE and HREE. CM harzburgites are enriched in LREE relative to MREE with 12 harzburgites that are depleted in LREE relative to MREE and HREE; this is not expected for mantle residues after near-fractional partial melting (Godard et al., 1995, 2000, 2008; Gruau et al., 1998; Johnson & Dick, 1992; Johnson et al., 1990; Kelemen et al., 1997; Navon & Stolper, 1987; Prinzhofer & Allègre, 1985; Vernières et al., 1997). The linear REE patterns observed in CM harzburgites are similar to the main harzburgites mantle section REE patterns from Wadi Tayin described by Godard et al. (2000); these harzburgites have relatively homogeneous modal and major element compositions. The Maqsad diapir area harzburgites and Samail massif *cpx*-harzburgites display concave-upward and 'spoon-shaped' REE patterns respectively, these patterns are not observed in CM Wadi Tayin harzburgites. The Maqsad diapir has been interpreted as frozen–upwelling mantle that fed a former spreading centre (Ceuleneer et al., 1988). The concave-upward REE patterns and the higher Al_2O_3/CaO ratios and TiO_2 contents in the diapir harzburgites result from the feedback between deformation and melt percolation, and the *cpx*-harzburgites REE patterns and chemical characteristics are interpreted as a result of a cpx forming melt-rock reaction at decreasing melt mass (at near-solidus conditions) along the lithosphere-asthenosphere boundary (Godard et al., 2000).

Figure 9 shows the modal composition of CM1A, CM2B (harzburgites and carbonate-bearing harzburgites) and Nakhl-Samail-Wadi Tayin massif samples (harzburgites, Godard et al., 2000) plotted with two published melting models: model 1 represents the Niu (1997) polybaric melting model (1a) with and (1b) without excess ol; model 2 represents the Walter et al. (1995) isobaric melting at 11 (2a), 16 (2b) and 17 kbar (2c). The figure indicates that CM harzburgites could result

591 from high degrees of partial melting and melt extraction in the range of 15-30 % (e.g. Asimow et
592 al., 2001; Kelemen et al., 1990, 1992, 1995; Niu, 1997; Walter et al., 1995), as suggested by
593 Godard et al. (2000) for the main harzburgite section of the MORB-like, NW-SE paleo spreading
594 segment (Nakhl-Samail-Wadi Tayin massifs). This range is higher than melting degrees producing
595 MORB in present-day oceans (5-10 %; Langmuir et al., 1992) and high-Ti magmas such as those
596 forming the sheeted dyke complex and the MORB-like lava sequence in Oman (Godard et al.,
597 2006; Lippard et al., 1986). However, Niu (1997) and Dick & Natland (1996) have reconciled this
598 inconsistency by considering that abyssal peridotites represent only the shallowest part of the
599 mantle column affected by partial melting and therefore record the highest melting degrees. In
600 contrast, MORB are thought to represent integrated, mixed melt fractions from polybaric
601 decompression melting over 60-100 km at ascent melting column and therefore record average
602 melting degrees.

603 The linear REE patterns of some studied harzburgites do not show features of strong LREE
604 depletion, but most of the other CM harzburgites show U-shaped REE patterns, characterized by
605 LREE enrichment. This, together with the high (primary) proportion of ol (75-90 %) observed in
606 some samples, point to the fact that near fractional partial melting alone fails to explain the
607 harzburgite geochemical signatures along the CM cores. Vernières et al. (1997) noted that the
608 relatively unfractionated REE distribution may simply result from melt transport through the
609 melting peridotites, as an "open-system melting process". This process would result in a negative
610 correlation between LREE/HREE ratios and peridotite fertility, as commonly observed in other
611 ophiolites (e.g. Prinzhofer & Allègre, 1985). It results from the competition between the partial
612 melting continuously depleting the mantle residue on one hand and chromatographic effects
613 related to the melt extraction that enrich the residue in the most incompatible elements on the other
614 hand (e.g. Johnson et al., 1990; Navon & Stolper, 1987; Niu, 2004; Takazawa et al., 1992;
615 Spiegelman & Kelemen, 2003).
616
617 CM harzburgites show good correlations among Yb, Ti and Hf concentrations, indicating that the
618 variability in HREE was more likely controlled by the melting process rather than by the overprint
619 of melt-rock reaction processes (Fig. 8 n-o). We compared the linear REE patterns in CM
620 harzburgites to Vernières et al. (1997) plate model calculations performed by Godard et al. (2000),
621 who modeled trace elements in peridotites form the Nakhl-Samail-Wadi Tayin massifs to explore
622 whether the REE variations observed in the studied harzburgites resulted from reactive porous
623 flow at increasing melt mass, or from partial melting coupled with melt transport (Fig. 10). The
624 authors first simulated a standard incremental melting model (experiment a, Fig. 10a, Johnson et
625 al., 1990). Then, they simulated reactive porous flow at increasing melt mass in a second model
626 (experiment b, Fig. 10b). Experiment (a) produces strongly LREE-depleted peridotite residues,
627 quite different in shape from CM and other Oman harzburgites. This experiment does not provide
628 a better fit to the data when the presence of the trapped melt in the residue is included (Fig. 10c).
629 Experiment (b) produces peridotite residues moderately depleted in LREE and with a small amount
630 of trapped melt (0.5-1 %) (Fig. 10d). The linear REE patterns of harzburgites from Holes CM1A
631 and CM2B are similar to Nakhl-Samail-Wadi Tayin harzburgites of Godard et al. (2000) and well
632 reproduced by experiment (b). The model suggests that part of the studied harzburgites were
633 pervasively percolated by diffuse melt flow which affected their geochemical signature. However,
634 the presence of many dunite intervals at the top of the mantle section requires an orthopyroxene-
635 consuming reaction between the residual peridotites and infiltrated melts.
636

The CMTZ pure dunites from CM holes (Wadi Tayin massif) display two types of chondrite-normalized REE patterns: (1) U-shaped REE patterns; (2) Linear LREE-depleted or slightly concave-upward REE patterns with similar HREE, MREE and LREE concentrations, with slightly lower LREE and MREE concentrations compared to HREE in some samples. The CMTZ impregnated dunites display three types of chondrite-normalized REE patterns: (1) linear REE patterns; (2) U-shaped REE patterns; (3) concave-upward patterns characterized by a nearly flat slope of the HREE segment followed by a progressive depletion from MREE to LREE. The Maqsad mantle-crust transition zone pure dunites trace elements are characterized by U-shaped to concave-upward REE patterns (Godard et al., 2000; Rospabé et al., 2018a, 2019a), similar to Maqsad diapir harzburgites (Godard et al., 2000) and to CM mantle dunites and harzburgites trace element patterns but with larger range of LREE variations in Maqsad MTZ dunites compared to Wadi Tayin CMTZ (CM cores). Maqsad impregnated dunites described by Rospabé et al. (2018a, 2019a) are characterized by similar trace element patterns to CM impregnated dunites, varying between linear LREE-depleted to variably concave-upward trace element patterns. Maqsad MTZ pure and impregnated dunites have been interpreted as end-members that recorded different stage of an initially shared same igneous process (Rospabé et al., 2018a, 2019a). Boudier & Nicolas (1995) and Godard et al (2000) attest that Maqsad MTZ dunites are diapir harzburgites that were strongly modified by ol-forming melt-rock reactions at high melt/rock ratios. Furthermore, Rospabé et al. (2018a) argue that the pure dunites are residues left after extraction of a percolating melt, whereas the impregnated dunites correspond to a frozen stage before complete melt extraction.

Relatively good covariations are observed in CM dunites and harzburgites between Th and U, Nb and especially La (Fig. 8 h, j), whereas their concentrations are not correlated with the HREE. Following many previous works, we interpret these correlations as the result of melt/peridotite reaction contemporaneously with, and/or subsequent to, the partial melting event discussed above. The crust-mantle transition zone pure and impregnated dunites from CM Holes display similar REE patterns to the dunites and harzburgites in the mantle section, U-/V-shaped REE patterns (displayed by 11 pure dunites and 3 impregnated dunites from the CM, CMTZ) cannot be explained by a pure cumulate origin (Fig. 7a-b). Several studies argued that the LREE enrichment relative to MREE cannot be explained by REE partition coefficients between ol and melt (Frey et al., 1978; Hauri & Hart, 1995; Kelemen et al., 1993; Lee et al., 2007; McKenzie & O'Nions, 1991; Sun & Liang, 2014) and may better be explained by peridotite metasomatism as a result of melt-peridotite reactions (e.g. Agranier & Lee, 2007; Godard et al., 1995; Navon & Stolper, 1987; Vernières et al., 1997). Most CM harzburgites display U-shaped REE patterns (15 harzburgites and 8 carbonate-bearing harzburgites) characterized by a LREE-enrichment compared to the linear REE patterns (12 harzburgites), with strong LREE enrichments indicating extensive interaction with a pervasive melt (Fig. 7a-b; e.g. Gerbert-Gaillard, 2002; Godard et al., 2000; Monnier et al., 2006). CM samples, in particular in Hole CM2B, show downhole variations that indicate a decreasing degree of melting with increasing depth (see Section 4.2.1. below geochemical logs). Two intervals from 170 m to 260 m, and 230 m to 300 m depth, are particularly good examples of this (Fig. 6, CM2B e.g. LREE, La, U). The correlations observed between LREE enrichment and an increasing fraction of trapped melt - calculated from experiment (b and d) in the most residual peridotites from 'Plate model' of Vernières et al. (1997) applied by Godard et al. (2000) (experiment b and d, see Fig.10) - in CM samples (e,g, La, Fig. 6), suggest that CM samples have

experienced extensive interaction with a pervasive melt or fluid (for fluid-melt-rock interactions at Maqsad CMTZ see also Rospabé et al. 2017, 2018a, 2019a). In the mantle section sampled by the CM cores, crosscutting dunites are widespread and represent end products of the opx-consuming reaction. The harzburgites experienced a more extensive melt flow at a shallow level that contributed to their ol enrichment (Fig. 1e, logs). The dunites were probably individualized by channeled percolation at the top of the melting column.

4.3. Petrological and geochemical overview of the mantle-crust transition in the SE of the Oman ophiolite

The CM ultramafic rocks studied in this paper (Wadi Tayin) compared to previously studied Maqsad MTZ dunites and diapir harzburgites show that: (1) the dunites have a replacive origin, they are the products of melt-harzburgite reaction leading to the complete consumption of orthopyroxene and concomitant precipitation of ol (e.g. Abily & Ceuleneer, 2013; Boudier & Nicolas, 1995; Gerbert-Gaillard, 2002; Godard et al., 2000; Kelemen et al., 1995, 1997; Koga et al., 2001; Rabinowicz et al., 1987; Rospabé et al., 2018a, and references therein). (2) The alternations between dunites and mantle harzburgites observed at the top of the mantle sequence of CM Holes were also observed at the base of the crust-mantle transition in many other massifs along the Oman ophiolite (e.g. Boudier & Nicolas, 1995), recording a snapshot of melt/harzburgite reaction frozen at the time of the uppermost mantle dunitization. (3) The vertical chemical trend changes related to the focus of the percolation/migration along faults observed at CM Holes samples have been previously observed at the Maqsad CMTZ dunites, with the same characteristic thickness of about 50 m (Rospabé et al. 2019a, 2020), confirming the control of synmagmatic faulting on melt/peridotite (± fluids) reactions and the petrological and geochemical structuration of the CMTZ.

The two main differences with the crust-mantle transition and mantle section of the neighboring Maqsad area, that have been extensively studied due to their diapir-related features (Ceuleneer et al., 1988), are that (1) if the two sites (Maqsad and OmanDP CM) are both more or less related to the rise of the mantle diapir, the CM site may have had less pronounced magmatic activity due to its distance to the axis of the diapir, and (2) the CM site may have been contaminated by possible remelting of the base of the old lithosphere during the development of the MORB segment, as evidenced in the Sumail massif at the borders of the area influenced by the diapir (Amri et al., 1996; Benoit et al., 1999; Clénet et al., 2010). In cores from Holes CM1A and CM2B, core description revealed the widespread presence of magmatic impregnations in the dunites (i.e. minerals that crystallized interstitially between ol grains during melt migration; e.g. Benn et al., 1988; Dick, 1989), and of magmatic segregation or more intruding dikes (Kelemen et al., 2020a, 2020b). This evidence for melt migration was described within both the crust-mantle transition and the mantle sequence. The impregnations in dunites are composed of plagioclase and clinopyroxene, and the magmatic segregations and dikes are mostly troctolitic and gabbroic, consistent with a MORB-like parent melt produced by decompression melting in the mantle. On the other hand, more exotic websterite and anorthositic gabbros to anorthosites were also observed in the mantle sequence and the dunite/harzburgite alternations.

CM ultramafic rocks studied in this paper (Wadi Tayin) show thus multiple differences compared to the previously studied Maqsad CMTZ dunites and diapir harzburgites: (1) the CM samples have

been more intensively affected by low temperature alteration features (serpentinization up to 100% in many samples). (2) The crust-mantle transition zone is thinner along CM drilled Holes (~150 m, Kelemen et al., 2020a, 2020b) compared to the Maqsad CMTZ (300-400 m, Abily and Ceuleneer, 2013, Boudier and Nicolas, 1995; Jousselin and Nicolas, 2000; Rabinowicz et al., 1987; Rospabé, 2018; Rospabé et al., 2019a). (3) CM pure dunites display lower LREE enrichements compared to the Maqsad ones. (4) Two major trends are observed in the trace element signatures of CM dunites and harzburgites, with good correlations between the Th and U, Nb and LREE on one hand, and between the HREE, Ti and Hf on the other hand, that are not observed at Maqsad. (5) The CM site CMTZ is mostly composed of pure dunites at the top and impregnated dunites at the bottom, whereas the typical structuration of the Maqsad CMTZ is generally composed by impregnated dunites at the top and pure dunites at the bottom (Rospabé, 2018; Rospabé et al. 2019a). (6) The dunites' impregnation characteristic appears to be different in Maqsad (e.g., mostly plagioclase and clinopyroxene (Boudier and Nicolas, 1995; Koga et al., 2001; Abily and Ceuleneer, 2013) but also widespread opx and amphibole impregnations in the higher level of the transition zone (Rospabé et al., 2017, 2018a, 2019a) compared to CM Hole dunites (plagioclase and clinopyroxene impregnations only). Similarly, exotic silicate inclusions (opx, amph, mica for the more abundant) enclosed in disseminated chromite grains in the dunites from the Maqsad area as well as in associated chromitite ore bodies (Lorand and Ceuleneer, 1989; Leblanc and Ceuleneer, 1991; Schiano et al., 1997; Borisova et al., 2012; Rollinson et al., 2018; Zagrtdenov et al., 2018; Rospabé et al., 2019b; 2020, 2021), suggest the involvement of a fluid or fluid-rich melt in the melt/rock reactions, which were not investigated in existing work on cores CM1A and CM2B - a few chromite schlierens have been sampled along the cores but not studied in details yet. Further investigation of CM ultramafic rock mineral chemistry is need to evaluate these discrepancies between the two CM and Maqsad sites.

All the above similarities and differences between CM Wadi Tayin and Maqsad ultramafic rocks point to a lighter imprint of melt-rock reaction at CM compared to Maqsad (e.g., thinner transition zone, lighter LREE enrichment in dunites, two distinct geochemical trends in trace elements, that perhaps are totally overprinted by stronger melt/rock reaction at Maqsad). This could be the consequence of one or the several factors: It could be related to the structural position of Wadi Tayin (at the periphery of the diapir) and Maqsad (centered on the diapir) leading to different melt/rock ratios (i.e., the geological context), to the timing of the occurrence of the melt-rock interaction, and/or to the nature of the percolating magma/fluid involved in the melt-rock reactions. Further detailed mineral chemistry, trace element geochemical modelling, structural and microstructural studies will be of use for addressing the above questions.

Conclusions

Continuous sampling of the Oman crust-mantle transition zone at Holes CM1A and CM2B, recovered by the Oman Drilling Project allows the study of the large range of petrological and geochemical variations in Oman ultramafic rocks with an unprecedented high resolution. Volatile (H_2O and CO_2), and major and trace elements of 56 dunites and 49 harzburgites from Holes CM1A and CM2B have been analyzed. CM1A and CM2B volatile element contents reflect extensive serpentinization (+/- carbonation) linked to the late-stage interaction with H_2O- and/or CO_2-bearing fluids. The refractory samples are characterized by relatively homogeneous modal and major element compositions, whereas other samples show primary cryptic and modal refertilization. Bulk rock Mg, Si and Al systematics and normative mineral modes suggest that

open system behavior during alteration (Mg loss and/or Si gain) affected many samples. However, the trace element concentrations are interpreted as reflecting magmatic processes and exhibit significant variations: the refractory harzburgites characterized by linear REE patterns are interpreted as mantle residues after ≥ 15 % melt extraction. The REE signatures in these samples can be explained by melt transport associated with partial melting. Other harzburgites displaying U-/V-shaped REE patterns are interpreted as the result of interstitial melt percolation. The pure and impregnated dunites from the mantle and the crust-mantle transition zones are characterized by similar trace element patterns as the mantle harzburgites, they are interpreted as reflecting different stages of ol-forming melt/rock reactions at high melt/rock ratio. The plagioclase and pyroxene minerals present in impregnated dunites indicate that the impregnated dunites represent the stage before complete extraction of the melt from the dunites, whereas the pure dunites represent the melt/rock reaction end-product after complete melt extraction (i.e. compaction of the ol matrix and system closure before/without interstitial plagioclase and clinopyroxene crystallization).

Acknowledgments

This research used samples and/or data provided by the Oman Drilling Project. The Oman Drilling Project (OmanDP) were funded from the International Continental Scientific Drilling Project (ICDP; Kelemen, Matter, Teagle Lead PIs), the Sloan Foundation-Deep Carbon Observatory (Grant 2014–3–01, Kelemen PI), the National Science Foundation (NSF–EAR–1516300, Kelemen lead PI), NASA–Astrobiology Institute (NNA15BB02A, Templeton PI), the German Research Foundation (DFG: KO 1723/21–1, Koepke PI), the Japanese Society for the Promotion of Science (JSPS no:16H06347, Michibayashi PI; and KAKENHI 16H02742, Takazawa PI), the European Research Council (Adv: no.669972; Jamveit PI), the Swiss National Science Foundation (SNF:20FI21_163073, Früh–Green PI), JAMSTEC, the TAMU–JR Science Operator, and contributions from the Sultanate of Oman Ministry of Regional Municipalities and Water Resources, the Oman Public Authority of Mining, Sultan Qaboos University, CRNS–Univ. Montpellier II, Columbia University of New York, and the University of Southampton. K.W is grateful for receiving the National Science Council, Taiwan (NSC-CDA-107-2628-M-001-006-MY4) and Academia Sinica, Taiwan (AS-CDA-107-M01) funds. F.K.'s participation in shipboard and onsite logging was supported by The Institute of earth science Academia Sinica, Taiwan and by the research grants awarded to K. Michibayashi by the Japan Society for the Promotion of Science (Kiban-B 16340151, Kiban-B 19340148 and Kiban-A 22244062).

Data Availability Statement

The dataset is available on the PANGAEA data archiving platform (https://doi.org/10.1594/PANGAEA.942402).

References

Abily, B., Ceuleneer, G., & Launeau, P. (2011). Synmagmatic normal faulting in the lower oceanic crust: Evidence from the Oman ophiolite. *Geology*, *39*(4), 391-394.

Abily, B., & Ceuleneer, G. (2013). The dunitic mantle-crust transition zone in the Oman ophiolite: Residue of melt-rock interaction, cumulates from high-MgO melts, or both?. *Geology, 41*(1), 67-70. https://doi.org/10.1130/G33351.1

Abily, B., Ceuleneer, G., Rospabé, M., Kaczmarek, M. A., Python, M., Grégoire, M., Benoit, M., & Rioux, M. (2021). Ocean crust accretion along a high-temperature detachment fault in the Oman ophiolite: A structural and petrological study of the Bahla massif. Tectonophysics, 229160. https://doi.org/10.1016/j.tecto.2021.229160

Agranier, A., & Lee, C. T. A. (2007). Quantifying trace element disequilibria in mantle xenoliths and abyssal peridotites. *Earth and Planetary Science Letters, 257*(1-2), 290-298. https://doi.org/10.1016/j.epsl.2007.02.041

Amri, I., Benoit, M., & Ceuleneer, G. (1996). Tectonic setting for the genesis of oceanic plagiogranites: evidence from a paleo-spreading structure in the Oman ophiolite. *Earth and Planetary Science Letters*, *139*(1-2), 177–194. https://doi.org/10.1016/0012-821X(95) 00233- 3.

Asimow, Paul D., M. M. Hirschmann, and E. M. Stolper. "Calculation of peridotite partial melting from thermodynamic models of minerals and melts, IV. Adiabatic decompression and the composition and mean properties of mid-ocean ridge basalts." *Journal of Petrology* 42.5 (2001): 963-998.

Barrat, J. A., Zanda, B., Moynier, F., Bollinger, C., Liorzou, C., & Bayon, G. (2012). Geochemistry of CI chondrites: Major and trace elements, and Cu and Zn isotopes. *Geochimica et Cosmochimica Acta, 83*, 79-92.

Barth, M. G., Mason, P. R., Davies, G. R., Dijkstra, A. H., & Drury, M. R. (2003). Geochemistry of the Othris ophiolite, Greece: evidence for refertilization?. *Journal of Petrology*, *44*(10), 1759-1785.

Batanova, V. G., Suhr, G., & Sobolev, A. V. (1998). Origin of geochemical heterogeneity in the mantle peridotites from the Bay of Islands ophiolite, Newfoundland, Canada: ion probe study of clinopyroxenes. *Geochimica et Cosmochimica Acta, 62*(5), 853-866. https://doi.org/10.1016/S0016-7037(97)00384-0

Batanova, V. G., & Savelieva, G. N. (2009). Melt migration in the mantle beneath spreading zones and formation of replacive dunites: a review. *Russian Geology and Geophysics, 50*(9), 763-778. https://doi.org/10.1016/j.rgg.2009.08.008

Bedini, R. M., & Bodinier, J. L. (1999). Distribution of incompatible trace elements between the constituents of spinel peridotite xenoliths: ICP-MS data from the East African Rift. *Geochimica et Cosmochimica Acta, 63*(22), 3883-3900. https://doi.org/10.1016/S0016-7037(99)00154-4

Beinlich, A., Plümper, O., Boter, E., Müller, I. A., Kourim, F., Ziegler, M., et al. (2020). Ophiolite carbonation: Constraints from listvenite core BT1B, Oman Drilling Project. Journal of Geophysical Research: Solid Earth, 125, e2019JB019060.

Benn, K., Nicolas, A., & Reuber, I. (1988). Mantle—crust transition zone and origin of wehrlitic magmas: Evidence from the Oman ophiolite. *Tectonophysics, 151*(1-4), 75-85. https://doi.org/10.1016/0040-1951(88)90241-7

Benoit, M., Polvé, M., & Ceuleneer, G. (1996). Trace element and isotopic characterization of mafic cumulates in a fossil mantle diapir (Oman ophiolite). *Chemical Geology*, *134*(1-3), 199-214. https://doi.org/10.1016/S0009-2541(96)00087-3

Benoit, M., Ceuleneer, G., & Polvé, M. (1999). The remelting of hydrothermally altered peridotite at mid-ocean ridges by intruding mantle diapirs. *Nature*, *402*(6761), 514-518. https://doi.org/10.1038/990073

Bodinier, J. L., Vasseur, G., Vernieres, J., Dupuy, C., & Fabries, J. (1990). Mechanisms of mantle metasomatism: geochemical evidence from the Lherz orogenic peridotite. *Journal of Petrology*, *31*(3), 597-628. https://doi.org/10.1093/petrology/31.3.597

Boudier, F., & Coleman, R. G. (1981). Cross section through the peridotite in the Samail ophiolite, southeastern Oman Mountains. *Journal of Geophysical Research: Solid Earth*, *86*(B4), 2573-2592. https://doi.org/10.1029/JB086iB04p02573

Boudier, F., & Nicolas, A. (1995). Nature of the Moho transition zone in the Oman ophiolite. *Journal of Petrology*, *36*(3), 777-796. https://doi.org/10.1093/petrology/36.3.777

Borisov, A. Y., Ceuleneer, G., Kamenetsky, V. S., Arai, S., Béjina, F., Abily, B., Bindeman, I. N., Polvé, M., De Parseval, P., Aigouy, T. Pokrovski, G. S. (2012). A new view on the petrogenesis of the Oman ophiolite chro- mitites from microanalyses of chromite-hosted inclusions. Journal of Petrology 53, 2411–2440.

Braun, M. G., & Kelemen, P. B. (2002c). Dunite distribution in the Oman ophiolite: Implications for melt flux through porous dunite conduits. *Geochemistry, Geophysics, Geosystems*, *3*(11), 1-21.

Ceuleneer, G., & Nicolas, A. (1985). Structures in podiform chromite from the Maqsad district (Samail ophiolite, Oman). *Mineralium Deposita*, *20*(3), 177-184. https://doi.org/10.1007/BF00204562

Ceuleneer, G., Nicolas, A., & Boudier, F. (1988). Mantle flow patterns at an oceanic spreading centre: the Oman peridotites record. *Tectonophysics*, *151*(1-4), 1-26. https://doi.org/10.1016/0040-1951(88)90238-7

Ceuleneer, G. (1991). Evidence for a paleo-spreading center in the Oman ophiolite: mantle structures in the Maqsad area. In *Ophiolite genesis and evolution of the oceanic lithosphere* (pp. 147-173). Springer, Dordrecht.

Ceuleneer, G., Monnereau, M., & Amri, I. (1996). Thermal structure of a fossil mantle diapir inferred from the distribution of mafic cumulates. *Nature*, *379*(6561), 149-153. https://doi.org/10.1038/379149a0

Clénet, H., Ceuleneer, G., Pinet, P., Abily, B., Daydou, Y., Harris, E., Amri, I., & Dantas, C. (2010). Thick sections of layered ultramafic cumulates in the Oman ophiolite revealed by an airborne hyperspectral survey: petrogenesis and relationship to mantle diapirism. *Lithos*, *114*(3-4), 265-281. https://doi.org/10.1016/j.lithos.2009.09.002

Dalton, H. B., Scott, J. M., Liu, J., Waight, T. E., Pearson, D. G., Brenna, M., ... & Palin, J. M. (2017). Diffusion-zoned pyroxenes in an isotopically heterogeneous mantle lithosphere

beneath the Dunedin Volcanic Group, New Zealand, and their implications for intraplate alkaline magma sources. *Lithosphere, 9*(3), 463-475. https://doi.org/10.1130/L631.1

de Obeso, J. C., & Kelemen, P. B. (2018). Fluid rock interactions on residual mantle peridotites overlain by shallow oceanic limestones: Insights from Wadi Fins, Sultanate of Oman. *Chemical Geology*, *498*, 139-149.

Dick, H. J. B. "Abyssal peridotites, very slow spreading ridges and ocean ridge magmatism." *Geological Society, London, Special Publications* 42.1 (1989): 71-105.

Dick, H. J., & Natland, J. H. (1996). Late-stage melt evolution and transport in the shallow mantle beneath the East Pacific Rise. In *Proceedings-Ocean Drilling Program Scientific Results (pp. 103-134)*. National Science Foundation.

Dygert, N., Liang, Y., & Kelemen, P.B. (2016). Formation of Plagioclase Lherzolite and Associated Dunite-Harzburgite-Lherzolite Sequences by Multiple Episodes of Mlet Percolation and Melt-Rock Reaction: an Example from the Trinity Ophiolite, California, USA. *Journal of Petrology*, *57*(4), 815-838.

Dygert, N., Kelemen, P.B., & Liang, Y. (2017) Spatial variations in cooling rate in the mantle section of the Samail ophiolite in Oman: Implications for the formation of lithosphere at mid-ocean ridges. *Earth and Planetary Science Letters*, *465*, 134-144.

Elthon, D. (1979). High magnesia liquids as the parental magma for ocean floor basalts. *Nature, 278*(5704), 514-518. https://doi.org/10.1038/278514a0

Fitzpayne, A., Giuliani, A., Hergt, J., Phillips, D., & Janney, P. (2018). New geochemical constraints on the origins of MARID and PIC rocks: Implications for mantle metasomatism and mantle-derived potassic magmatism. *Lithos, 318*, 478-493. https://doi.org/10.1016/j.lithos.2018.08.036

Frey, F. A., Green, D. H., & Roy, S. D. (1978). Integrated models of basalt petrogenesis: a study of quartz tholeiites to olivine melilitites from south eastern Australia utilizing geochemical and experimental petrological data. *Journal of petrology, 19*(3), 463-513. https://doi.org/10.1093/petrology/19.3.463

Gerbert-Gaillard L. (2002). Caractérisation géochimique des péridotites de l'ophiolite d'Oman : processus magmatiques aux limites lithosphère/asthénosphère. PhD Thesis Université Montpellier II - Sciences et Techniques du Languedoc, 238 pp.

Girardeau, J., Monnier, C., Le Mée, L., & Quatrevaux, F. (2002). The Wuqbah peridotite, central Oman ophiolite: petrological characteristics of the mantle in a fossil overlapping ridge setting. *Marine Geophysical Researches*, *23*(1), 43-56. https://doi.org/10.1023/A:1021297614067

Glennie, K., Boeuf, M. G. A., Hughes Clarke, M. W., Moody-Stuart, M., Pilaar, W. F. H. & Reinhardt, B. M. (1974). The geology of the Oman Mountains. *Verhandelingen van het Koninklijk Nederlands Geologisch Mijnbouwkundig Genootschap*, *31*, 423pp.

Godard, M., Bodinier, J. L., & Vasseur, G. (1995). Effects of mineralogical reactions on trace element redistributions in mantle rocks during percolation processes: a chromatographic approach. *Earth and Planetary Science Letters, 133*(3), 449-462. https://doi.org/10.1016/0012-821X(95)00104-K

Godard, M., Jousselin, D., & Bodinier, J. L. (2000). Relationships between geochemistry and structure beneath a palaeo-spreading centre: a study of the mantle section in the Oman ophiolite. *Earth and Planetary Science Letters*, *180*(1-2), 133-148. https://doi.org/10.1016/S0012-821X(00)00149-7

Godard, M., Bosch, D., & Einaudi, F. (2006). A MORB source for low-Ti magmatism in the Semail ophiolite. *Chemical geology*, *234*(1-2), 58-78. https://doi.org/10.1016/j.chemgeo.2006.04.005

Godard, M., Lagabrielle, Y., Alard, O., & Harvey, J. (2008). Geochemistry of the highly depleted peridotites drilled at ODP Sites 1272 and 1274 (Fifteen-Twenty Fracture Zone, Mid-Atlantic Ridge): Implications for mantle dynamics beneath a slow spreading ridge. *Earth and Planetary Science Letters*, *267*(3-4), 410-425. https://doi.org/10.1016/j.epsl.2007.11.058

Grégoire, M., McInnes, B. I., & O'Reilly, S. Y. (2001). Hydrous metasomatism of oceanic sub-arc mantle, Lihir, Papua New Guinea: Part 2. Trace element characteristics of slab-derived fluids. *Lithos, 59*(3), 91-108. https://doi.org/10.1016/S0024-4937(01)00058-5

Gruau, G., Bernard-Griffiths, J., & Lécuyer, C. (1998). The origin of U-shaped rare earth patterns in ophiolite peridotites: assessing the role of secondary alteration and melt/rock reaction. *Geochimica et Cosmochimica Acta, 62*(21-22), 3545-3560. https://doi.org/10.1016/S0016-7037(98)00250-6

Hanghøj, K., Kelemen, P. B., Hassler, D., & Godard, M. (2010). Composition and genesis of depleted mantle peridotites from the Wadi Tayin Massif, Oman Ophiolite; major and trace element geochemistry, and Os isotope and PGE systematics. *Journal of Petrology*, 51(1-2), 201-227. https://doi.org/10.1093/petrology/egp077

Hauri, E. H., Hart, S. R. (1995). Correction to 'Constraints on melt migration from mantle plumes: a trace element study of peridotite xenoliths from Savai'i, Western Samoa'. *Journal of Geophysical Research*, 100, 2003-2003.

Hodel, F., Macouin, M., Trindade, R. I. F., Triantafyllou, A., Ganne, J., Chavagnac, V., Berger, J., Rospabé, M., Destrigneville, C., Carlut, J., Ennih, N., & Ennih, N. (2018). Fossil black smoker yields oxygen isotopic composition of Neoproterozoic seawater. *Nature communications, 9*(1), 1-7. https://doi.org/10.1038/s41467-018-03890-w

Ionov, D. A., Savoyant, L., & Dupuy, C. (1992). Application of the ICP-MS technique to trace element analysis of peridotites and their minerals. *Geostandards Newsletter, 16*(2), 311-315. https://doi.org/10.1111/j.1751-908X.1992.tb00494.x

Hopson, C. A., Coleman, R. G., Gregory, R. T., Pallister, J. S., & Bailey, E. H. (1981). Geologic section through the Samail ophiolite and associated rocks along a Muscat-Ibra transect, southeastern Oman Mountains. *Journal of Geophysical Research: Solid Earth, 86*(B4), 2527-2544.

Jagoutz, E., Palme, H., Baddenhausen, H., Blum, K., Cendales, M., Dreibus, G., Spettel, B., Lorenz, V. and Wanke, H. (1979). The abundances of major, minor and trace elements in the earth's mantle as derived from primitive ultramafic nodules. Proc. Lunar Planet. Sci. Conf. 10th, 2031–2050.

971 Johnson, K. T., Dick, H. J., & Shimizu, N. (1990). Melting in the oceanic upper mantle: an ion
972 microprobe study of diopsides in abyssal peridotites. *Journal of Geophysical Research:*
973 *Solid Earth*, *95*(B3), 2661-2678. https://doi.org/10.1029/JB095iB03p02661

974 Johnson, K.T. & Dick, H. J. B. (1992). Open system melting and temporal and spatial variation of
975 peridotite and basalt at the Atlantis II fracture zone. Journal of Geophysical Research 97,
976 9219-241.

977 Jousselin, D., Nicolas, A., & Boudier, F. (1998). Detailed mapping of a mantle diapir below a
978 paleo-spreading center in the Oman ophiolite. *Journal of Geophysical Research: Solid*
979 *Earth*, *103*(B8), 18153-18170. https://doi.org/10.1029/98JB01493

980 Jousselin, D., & Nicolas, A. (2000). The Moho transition zone in the Oman ophiolite-relation with
981 wehrlites in the crust and dunites in the mantle. *Marine Geophysical Researches*, *21*(3-4),
982 229-241. https://doi.org/10.1023/A:1026733019682

983 Kanke, N., & Takazawa, E. (2014). A kilometre-scale highly refractory harzburgite zone in the
984 mantle section of the northern Oman Ophiolite (Fizh Block): implications for flux melting
985 of oceanic lithospheric mantle. *Geological Society, London, Special Publications*, *392*(1),
986 229-246. https://doi.org/10.1144/SP392.12

987 Kelemen, P. B., & Ghiorso, M. S. (1986). Assimilation of peridotite in zoned calc-alkaline plutonic
988 complexes: evidence from the Big Jim complex, Washington Cascades. *Contributions to*
989 *Mineralogy and Petrology*, *94*(1), 12-28.

990 Kelemen P. B. (1990) Reaction between ultramafic rock and fractionating basaltic magma I. phase
991 relations, the origin of calc-alkaline magma series, and the formation of discordant dunite.
992 J. Petrol. 31, 51–98.

993 Kelemen P. B., Dick H. J. B. and Quick J. E. (1992) Formation of harzburgite by pervasive
994 melt/rock reaction in the upper mantle. Nature 358, 635–641.

995 Kelemen, P. B., Shimizu, N., & Dunn, T. (1993). Relative depletion of niobium in some arc
996 magmas and the continental crust: partitioning of K, Nb, La and Ce during melt/rock
997 reaction in the upper mantle. *Earth and Planetary Science Letters*, *120*(3-4), 111-134.
998 https://doi.org/10.1016/0012-821X(93)90234-Z

999 Kelemen, P. B., Shimizu, N., & Salters, V. J. (1995). Extraction of mid-ocean-ridge basalt from
1000 the upwelling mantle by focused flow of melt in dunite channels. *Nature*, *375*(6534), 747-
1001 753. https://doi.org/10.1038/375747a0

1002 Kelemen, P. B., Hirth, G., Shimizu, N., Spiegelman, M., & Dick, H. J. (1997). A review of melt
1003 migration processes in the adiabatically upwelling mantle beneath oceanic spreading
1004 ridges. *Philosophical Transactions of the Royal Society of London. Series A:*
1005 *Mathematical, Physical and Engineering Sciences*, *355*(1723), 283-318.
1006 https://doi.org/10.1098/rsta.1997.0010

1007 Kelemen, P. B., Hart, S. R., & Bernstein, S. (1998). Silica enrichment in the continental upper
1008 mantle via melt/rock reaction. *Earth and Planetary Science Letters*, *164*(1-2), 387-406.
1009 https://doi.org/10.1016/S0012-821X(98)00233-7

1010 Kelemen, P.B., Matter, J.M., Teagle, D.A.H., Coggon, J.A., and the Oman Drilling Project Science
1011 Team (2020a). Site CM1: layered gabbros, crustal ultramafic rocks, and mantle

harzburgite. In Kelemen, P.B., Matter, J.M., Teagle, D.A.H., Coggon, J.A., et al., Proceedings of the Oman Drilling Project: College Station, TX (International Ocean Discovery Program).

Kelemen, P.B., Matter, J.M., Teagle, D.A.H., Coggon, J.A., and the Oman Drilling Project Science Team (2020b, in press). Site CM2: crust-mantle transition zone and into upper mantle. In Kelemen, P.B., Matter, J.M., Teagle, D.A.H., Coggon, J.A., et al., Proceedings of the Oman Drilling Project: College Station, TX (International Ocean Discovery Program) doi:10.14379/OmanDP.proc.2020, 2021b.

Kelemen, P.B., Matter, J.M., Teagle, D.A.H., Coggon, J.A., and the Oman Drilling Project Science Team, 2020c. Methods and explanatory notes. *In* Kelemen, P.B., Matter, J.M., Teagle, D.A.H., Coggon, J.A., et al., *Proceedings of the Oman Drilling Project:* College Station, TX (International Ocean Discovery Program).

Khedr, M. Z., Arai, S., Python, M., & Tamura, A. (2014). Chemical variations of abyssal peridotites in the central Oman ophiolite: evidence of oceanic mantle heterogeneity. *Gondwana Research*, *25*(3), 1242-1262.

Koga, K. T., Kelemen, P. B., & Shimizu, N. (2001). Petrogenesis of the crust-mantle transition zone and the origin of lower crustal wehrlite in the Oman ophiolite. *Geochemistry, Geophysics, Geosystems*, *2*(9). https://doi.org/10.1016/j.gr.2013.05.010

Kogiso, T., Tatsumi, Y., & Nakano, S. (1997). Trace element transport during dehydration processes in the subducted oceanic crust: 1. Experiments and implications for the origin of ocean island basalts. *Earth and Planetary Science Letters*, *148*(1-2), 193-205.

Kourim, F., Bodinier, J. L., Alard, O., Bendaoud, A., Vauchez, A., & Dautria, J. M. (2014). Nature and evolution of the lithospheric mantle beneath the Hoggar swell (Algeria): a record from mantle xenoliths. *Journal of Petrology*, *55*(11), 2249-2280. https://doi.org/10.1093/petrology/egu056

Langmuir, C. H., Klein, E. M., & Plank, T. (1992). Petrological systematics of mid-ocean ridge basalts: Constraints on melt generation beneath ocean ridges. *Mantle flow and melt generation at mid-ocean ridges*, *71*, 183-280.

Leblanc, M. Ceuleneer, G. (1991). Chromite crystallization in a multicellular magma flow: Evidence from a chromitite dike in the Oman ophiolite. Lithos 27, 231–257.

Le Mée, L., Girardeau, J., & Monnier, C. (2004). Mantle segmentation along the Oman ophiolite fossil mid-ocean ridge. *Nature*, *432*(7014), 167-172. https://doi.org/10.1038/nature03075

Lee, C. T. A., Harbert, A., & Leeman, W. P. (2007). Extension of lattice strain theory to mineral/mineral rare-earth element partitioning: an approach for assessing disequilibrium and developing internally consistent partition coefficients between olivine, orthopyroxene, clinopyroxene and basaltic melt. *Geochimica et Cosmochimica Acta*, *71*(2), 481-496. https://doi.org/10.1016/j.gca.2006.09.014

Lippard, S. J., Shelton, A. W. & Gass, I. G. (1986). The ophiolite of northern Oman. *Geological Society London Memoir*, *11*, 178.

Lorand, J. P. (1988). Fe-Ni-Cu sulfides in tectonite peridotites from the Maqsad district, Sumail ophiolite, southern Oman: Implications for the origin of the sulfide component in the

oceanic upper mantle. *Tectonophysics*, 151(1-4), 57-73. https://doi.org/10.1016/0040-1951(88)90240-5

Lorand, J.-P. Ceuleneer, G. (1989). Silicate and base-metal sulfide inclusions in chromites from the Maqsad area (Oman ophiolite, Gulf of Oman): a model for entrapment. *Lithos* 22, 173–190. https://doi.org/10.1016/0024-4937(89)90054-6

Malvoisin B. (2015) Mass transfer in the oceanic lithosphere: serpentinization is not isochemical. *Earth and Planetary Science Letters*, *430*, 75–85. https://doi.org/10.1016/j.epsl.2015.07.043

McKenzie, Dan, & O'Nions, R. K. (1991). Partial melt distributions from inversion of rare earth element concentrations. *Journal of Petrology*, *32*(5), 1021-1091. https://doi.org/10.1093/petrology/32.5.1021

Monnier, C., Girardeau, J., Le Mée, L., & Polvé, M. (2006). Along-ridge petrological segmentation of the mantle in the Oman ophiolite. *Geochemistry, Geophysics, Geosystems*, *7*(11). https://doi.org/10.1029/2006GC001320

Morgan, Z., Liang, Y., & Kelemen, P.B. (2008). Significance of the concentration gradients associated with dunite bodies in the Josephine and Trinity ophiolites. *Geochemistry, Geophysics, Geosystems*, *9*(7). Doi:10.1029/2008GC001954.

Navon, O., & Stolper, E. (1987). Geochemical consequences of melt percolation: the upper mantle as a chromatographic column. *The Journal of Geology*, *95*(3), 285-307. https://doi.org/10.1086/629131

Nicolas, A., Ceuleneer, G., Boudier, F., & Misseri, M. (1988). Structural mapping in the Oman ophiolites: Mantle diapirism along an oceanic ridge. *Tectonophysics*, *151*(1-4), 27-56. https://doi.org/10.1016/0040-1951(88)90239-9

Nicolas, A., & Boudier, F. (1995). Mapping oceanic ridge segments in Oman ophiolite. *Journal of Geophysical Research: Solid Earth*, *100*(B4), 6179-6197.

Nicolas, A., Boudier, F., Ildefonse, B., & Ball, E. (2000). Accretion of Oman and United Arab Emirates ophiolite–discussion of a new structural map. *Marine Geophysical Researches*, *21*(3-4), 147-180. https://doi.org/10.1023/A:1026769727917

Nicolas, A., & Boudier, F. (2008). Large shear zones with no relative displacement. *Terra Nova*, *20*(3), 200-205. https://doi.org/10.1111/j.1365-3121.2008.00806.x

Nicolas, A. (2012). *Structures of ophiolites and dynamics of oceanic lithosphere* (Vol. 4). Springer Science & Business Media.

Niu, Y. (1997). Mantle melting and melt extraction processes beneath ocean ridges: evidence from abyssal peridotites. *Journal of Petrology*, *38*(8), 1047-1074. https://doi.org/10.1093/petroj/38.8.1047

Niu Y. (2004) Bulk-rock major and trace element compositions of abyssal peridotites: implications for mantle melting, melt extraction and post-melting processes beneath Mid-Ocean ridges. J. Petrol. 45, 2423–2458.

O'Hara, M. J. (1965). Primary magmas and the origin of basalts. *Scottish Journal of Geology*, *1*(1), 19-40. https://doi.org/10.1144/sjg01010019

Oliveira, B., Afonso, J. C., & Tilhac, R. (2020). A disequilibrium reactive transport model for mantle magmatism. *Journal of Petrology*.

Parkinson, I. J., & Pearce, J. A. (1998). Peridotites from the Izu–Bonin–Mariana forearc (ODP Leg 125): evidence for mantle melting and melt–mantle interaction in a supra-subduction zone setting. *Journal of Petrology, 39*(9), 1577-1618. https://doi.org/10.1093/petroj/39.9.1577

Paulick, H., Bach, W., Godard, M., De Hoog, J. C. M., Suhr, G., & Harvey, J. (2006). Geochemistry of abyssal peridotites (Mid-Atlantic Ridge, 15 20′ N, ODP Leg 209): implications for fluid/rock interaction in slow spreading environments. *Chemical geology, 234(3-4)*, 179-210. https://doi.org/10.1016/j.chemgeo.2006.04.011

Prinzhofer, A., & Allègre, C. J. (1985). Residual peridotites and the mechanisms of partial melting. *Earth and Planetary Science Letters, 74*(2-3), 251-265. https://doi.org/10.1016/0012-821X(85)90025-1

Python, M., & Ceuleneer, G. (2003). Nature and distribution of dykes and related melt migration structures in the mantle section of the Oman ophiolite. *Geochemistry, Geophysics, Geosystems*, *4*(7). https://doi.org/10.1029/2002GC000354

Python, M., Ceuleneer, G., & Arai, S. (2008). Chromian spinels in mafic–ultramafic mantle dykes: evidence for a two-stage melt production during the evolution of the Oman ophiolite. *Lithos*, *106*(1-2), 137-154. https://doi.org/10.1016/j.lithos.2008.07.001

Quick, J. E. (1981a). Petrology and petrogenesis of the Trinity Peridotite, an upper mantle diapir in the Eastern Klamath Mountains, Northern California. *Journal of Geophysical Research: Solid Earth 86*(B12), 11837–11863. https://doi.org/10.1029/JB086iB12p11837

Quick, J. E. (1981b). The origin and significance of large, tabular dunite bodies in the Trinity peridotite, northern California. *Contributions to Mineralogy and Petrology 78*(4), 413–422. https://doi.org/10.1007/BF00375203

Rabinowicz, M., Ceuleneer, G., & Nicolas, A. (1987). Melt segregation and flow in mantle diapirs below spreading centers: evidence from the Oman ophiolite. *Journal of Geophysical Research: Solid Earth*, *92*(B5), 3475-3486. https://doi.org/10.1029/JB092iB05p03475

Rioux, M., Bowring, S., Kelemen, P., Gordon, S., Miller, R., & Dudás, F. (2013). Tectonic development of the Samail ophiolite: High-precision U-Pb zircon geochronology and Sm-Nd isotopic constraints on crustal growth and emplacement. *Journal of Geophysical Research: Solid Earth*, *118*(5), 2085-2101. https://doi.org/10.1002/jgrb.50139

Rioux, M., Bowring, S., Kelemen, P., Gordon, S., Dudás, F., & Miller, R. (2012). Rapid crustal accretion and magma assimilation in the Oman-UAE ophiolite: High precision U-Pb zircon geochronology of the gabbroic crust. *Journal of Geophysical Research: Solid Earth*, *117*(B7). https://doi.org/10.1029/2012JB009273

Rioux, M., Garber, J., Bauer, A., Bowring, S., Searle, M., Kelemen, P., & Hacker, B. (2016). Synchronous formation of the metamorphic sole and igneous crust of the Semail ophiolite: New constraints on the tectonic evolution during ophiolite formation from high-precision U–Pb zircon geochronology. *Earth and Planetary Science Letters*, *451*, 185-195. https://doi.org/10.1016/j.epsl.2016.06.051

Rollinson, H., Mameri, L. Barry, T. (2018). Polymineralic inclusions in mantle chromitites from the Oman ophiolite indicate a highly magnesian parental melt. Lithos 310–311, 381–391.

Rospabé, M., Ceuleneer, G., Benoit, M., Abily, B., & Pinet, P. (2017). Origin of the dunitic mantle-crust transition zone in the Oman ophiolite: The interplay between percolating magmas and high-temperature hydrous fluids. *Geology*, *45*(5), 471-474. https://doi.org/10.1130/G38778.1

Rospabé, M. (2018). Etude pétrologique, géochimique et structurale de la zone de transition dunitique dans l'ophio- lite d'Oman : Identification des processus pétrogénétiques à l'interface manteau/croûte. PhD thesis, Université Paul Sabatier, Toulouse III, 628 pp.

Rospabé, M., Benoit, M., Ceuleneer, G., Hodel, F., & Kaczmarek, M. A. (2018a). Extreme geochemical variability through the dunitic transition zone of the Oman ophiolite: implications for melt/fluid-rock reactions at Moho level beneath oceanic spreading centers. *Geochimica et cosmochimica acta*, *234*, 1-23. https://doi.org/10.1016/j.gca.2018.05.012

Rospabé, M., Benoit, M., & Candaudap, F. (2018b). Determination of trace element mass fractions in ultramafic rocks by HR-ICP-MS: A combined approach using a direct digestion/dilution method and preconcentration by coprecipitation. *Geostandards and Geoanalytical Research*, *42*(1), 115-129. https://doi.org/10.1111/ggr.12181

Rospabé, M., Benoit, M., Ceuleneer, G., Kaczmarek, M. A., & Hodel, F. (2019a). Melt hybridization and metasomatism triggered by syn-magmatic faults within the Oman ophiolite: A clue to understand the genesis of the dunitic mantle-crust transition zone. *Earth and Planetary Science Letters*, *516*, 108-121. https://doi.org/10.1016/j.epsl.2019.04.004

Rospabé, M., Ceuleneer, G., Granier, N., Arai, S.; Borisova, A. Y. (2019b). Multi-scale development of a stratiform chromite ore body at the base of the dunitic mantle–crust transition zone (Maqsad diapir, Oman ophiolite): the role of repeated melt and fluid influxes. Lithos 350–351, 105235.

Rospabé, M., Ceuleneer, G., Benoit, M., & Kaczmarek, M. A. (2020). Composition gradients in silicate inclusions in chromites from the dunitic mantle-crust transition (Oman ophiolite) reveal high temperature fluid-melt-rock interaction controlled by faulting. *Ofioliti. An international journal on ophiolites and oceanic lithosphere*, *45*(2), 103-114. https://doi.org/10.4454/ofioliti.v45i2.534

Rospabé, M., Ceuleneer, G., Le Guluche, V., Benoit, M., & Kaczmarek, M. A. (2021). The Chicken and Egg Dilemma Linking Dunites and Chromitites in the Mantle-Crust Transition Zone Beneath Oceanic Spreading Centres: A Case Study of Chromite-hosted Silicate Inclusions in Dunites Formed at the Top of a Mantle Diapir (Oman Ophiolite). *Journal of Petrology*.

Sauter, D., Werner, P., Ceuleneer, G., Manatschal, G., Rospabé, M., Tugend, J., ... & Ulrich, M. (2021). Sub-axial deformation in oceanic lower crust: Insights from seismic reflection profiles in the Enderby Basin and comparison with the Oman ophiolite. *Earth and Planetary Science Letters*, *554*, 116698.

Schiano, P., Clocchiatti, R., Lorand, J.-P., Massare, D., Deloule, E. Chaussidon, M. (1997). Primitive basaltic melts included in podiform chromites from the Oman Ophiolite. Earth and Planetary Science Letters 146, 489–497.

Searle, M. P., & Malpas, J. (1980). Structure and metamorphism of rocks beneath the Semail ophiolite of Oman and their significance in ophiolite obduction. *Earth and Environmental Science Transactions of the Royal Society of Edinburgh*, *71*(4), 247-262. https://doi.org/10.1017/S0263593300013614

Smewing, J. D. (1981). Mixing characteristics and compositional differences in mantle-derived melts beneath spreading axes: Evidence from cyclically layered rocks in the ophiolite of North Oman. *Journal of Geophysical Research: Solid Earth*, *86*(B4), 2645-2659. https://doi.org/10.1029/JB086iB04p02645

Snow, J. E., & Dick, H. J. (1995). Pervasive magnesium loss by marine weathering of peridotite. *Geochimica et Cosmochimica Acta, 59(20)*, 4219-4236. https://doi.org/10.1016/0016-7037(95)00239-V

Spiegelman, M., & Kelemen, P. B. (2003). Extreme chemical variability as a consequence of channelized melt transport. *Geochemistry, Geophysics, Geosystems*, *4*(7).

Sun, C., & Liang, Y. (2014). An assessment of subsolidus re-equilibration on REE distribution among mantle minerals olivine, orthopyroxene, clinopyroxene, and garnet in peridotites. *Chemical Geology*, *372*, 80-91. https://doi.org/10.1016/j.chemgeo.2014.02.014

Sun, S. S., & McDonough, W. F. (1989). Chemical and isotopic systematics of oceanic basalts: implications for mantle composition and processes. *Geological Society, London, Special Publications*, *42*(1), 313-345.

Takazawa, E., Frey, F. A., Shimizu, N., Obata, M., & Bodinier, J. L. (1992). Geochemical evidence for melt migration and reaction in the upper mantle. *Nature, 359*(6390), 55-58. https://doi.org/10.1038/359055a0

Takazawa, E., Okayasu, T., & Satoh, K. (2003). Geochemistry and origin of the basal lherzolites from the northern Oman ophiolite (northern Fizh block). *Geochemistry, Geophysics, Geosystems*, *4*(2). https://doi.org/10.1029/2001GC000232

Tilton, G. R., Hopson, C. A., & Wright, J. E. (1981). Uranium-lead isotopic ages of the Samail ophiolite, Oman, with applications to Tethyan ocean ridge tectonics. *Journal of Geophysical Research: Solid Earth*, *86*(B4), 2763-2775. https://doi.org/10.1029/JB086iB04p02763

Tippit, P. R., Pessagno, E. A., & Smewing, J. D. (1981). The biostratigraphy of sediments in the volcanic unit of the Samail ophiolite. *Journal of Geophysical Research: Solid Earth*, *86*(B4), 2756-2762. https://doi.org/10.1029/JB086iB04p02756

Tommasi, A., & Vauchez, A. (2015). Heterogeneity and anisotropy in the lithospheric mantle. *Tectonophysics, 661*, 11-37. https://doi.org/10.1016/j.tecto.2015.07.026

Vauchez, A., Dineur, F., & Rudnick, R. (2005). Microstructure, texture and seismic anisotropy of the lithospheric mantle above a mantle plume: insights from the Labait volcano xenoliths (Tanzania). *Earth and Planetary Science Letters, 232*(3-4), 295-314. https://doi.org/10.1016/j.epsl.2005.01.024

Vernières, J., Godard, M., & Bodinier, J. L. (1997). A plate model for the simulation of trace element fractionation during partial melting and magma transport in the Earth's upper mantle. *Journal of Geophysical Research: Solid Earth*, *102*(B11), 24771-24784. https://doi.org/10.1029/97JB01946

Walter, M. J., Sisson, T. W., & Presnall, D. C. (1995). A mass proportion method for calculating melting reactions and application to melting of model upper mantle lherzolite. *Earth and Planetary Science Letters*, *135*(1-4), 77-90. https://doi.org/10.1016/0012-821X(95)00148-6

Warren, C. J., Parrish, R. R., Waters, D. J., & Searle, M. P. (2005). Dating the geologic history of Oman's Semail ophiolite: Insights from U-Pb geochronology. *Contributions to Mineralogy and Petrology*, *150*(4), 403-422. https://doi.org/10.1007/s00410-005-0028-5

Warren, J.M., Shimizu, N., Skaaguchi, C., Dick, H.J.B., & Nakamura, E. (2009). An assessment of upper mantle heterogeneity based on abyssal peridotite isotopic compositions. *Journal of Geophysical Research*, *114*, B12203. doi:10.1029/2008JB006186.

Warren, J.B., & Shimizu, N. (2010). Cryptic Variations in Abyssal Peridotite Compositions: Evidence for Shallow-level Melt Infiltration in the Oceanic Lithosphere. *Journal of Petrology*, *51*(1-2), 395-423.

Yokoyama, T., Makishima, A., & Nakamura, E. (1999). Evaluation of the coprecipitation of incompatible trace elements with fluoride during silicate rock dissolution by acid digestion. *Chemical Geology*, *157*(3-4), 175-187.

Zagrtdenov, N. R., Ceuleneer, G., Rospabé, M., Borisova, A. Y., Toplis, M. J., Benoit, M.; Abily, B. (2018). Anatomy of a chromitite dyke in the mantle/crust transition zone of the Oman ophiolite. Lithos 312, 343–357.

1240 **Figure captions**

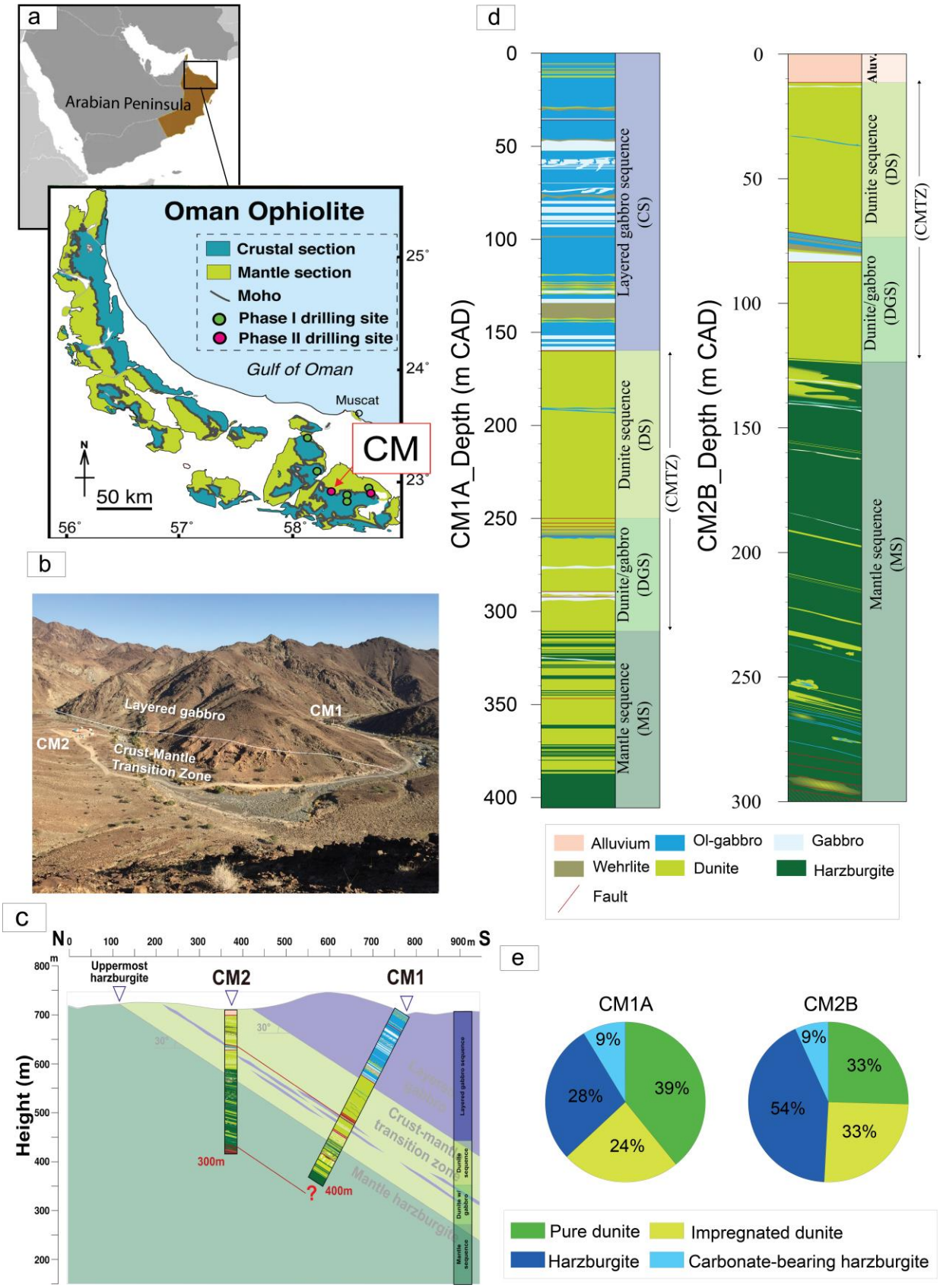
a
Arabian Peninsula
Oman Ophiolite
Crustal section
Mantle section
Moho
Phase I drilling site
Phase II drilling site
Gulf of Oman
Muscat
CM
25°
24°
23°
N
50 km
56°
57°
58°
b
Layered gabbro
CM1
CM2
Crust-Mantle
Transition Zone
c
N
S
0
100
200
300
400
500
600
700
800
900 m
Uppermost
harzburgite
CM2
CM1
Height (m)
800
700
600
500
400
300
200
30°
30°
300m
400m
?
Layered gabbro sequence
Crust-mantle transition zone
Mantle harzburgite
Dunite sequence
Dunite w/ gabbro
Mantle sequence
d
CM1A_Depth (m CAD)
0
50
100
150
200
250
300
350
400
Layered gabbro sequence (CS)
Dunite sequence (DS)
Dunite/gabbro (DGS)
Mantle sequence (MS)
(CMTZ)
CM2B_Depth (m CAD)
0
50
100
150
200
250
300
Aluv.
Dunite sequence (DS)
Dunite/gabbro (DGS)
Mantle sequence (MS)
(CMTZ)
Alluvium
Ol-gabbro
Gabbro
Wehrlite
Dunite
Harzburgite
Fault
e
CM1A
9%
28%
39%
24%
CM2B
9%
54%
33%
33%
Pure dunite
Impregnated dunite
Harzburgite
Carbonate-bearing harzburgite

1241

Figure 1 Geological context, **a** Simplified geological map showing the location of Holes CM1A and CM2B in the context of the regional and local geology (after Nicolas & Boudier, 1995). **b** Field photographs showing the location of Holes CM1A and CM2B. **c** Simplified N-S cross-section showing the different sampled lithologies and the correlation in depth between Holes CM1A and CM2B. **d** Downhole stratigraphy of CM1A and CM2B showing the distribution of the lithologies in the crust, crust-mantle and mantle sequences. **e** pie charts showing the studied samples lithology count in Hole CM1A and CM2B (see Section 3 in the Supporting Information).

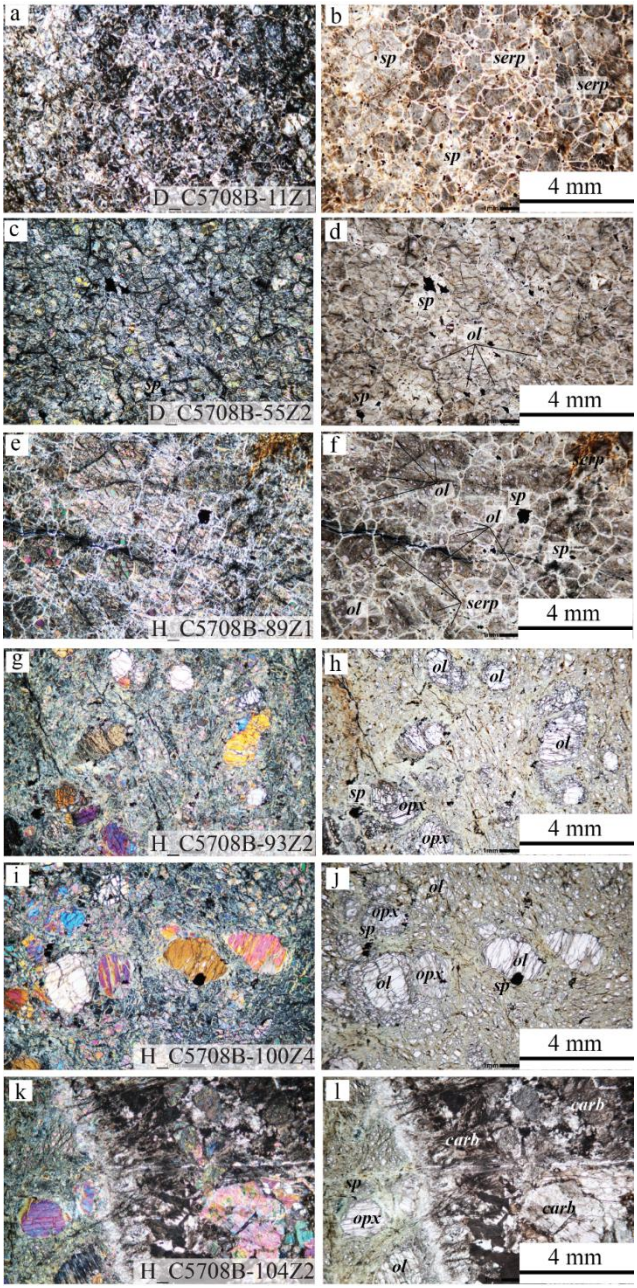

Figure 2 microphotographs of petrographic details of a selection of CMTZ dunites (**a, b, c** and **d)** and harzburgites (**e, f, g, h, i, j, k** and **l)** from Holes CM1A and CM2B. The dunites are characterized by fine- to medium grained granular texture and the harzburgites by porphyroclastic

texture. The dunites and harzburgites have generally preserved their primary high temperature texture (granular or porphyroclastic textures) after complete (**a,** and **b**), or partial (**c, d, e, f, g, h. i, j, k** and **l)** replacement of olivine crystals by serpentine. **i** and **j** illustrate microphotographs of a plastically deformed orthopyroxene surrounded by neoblasts. **k** and **l** show harzburgite CM2B-104Z2 crosscut by low-temperature veins (Carbonate).

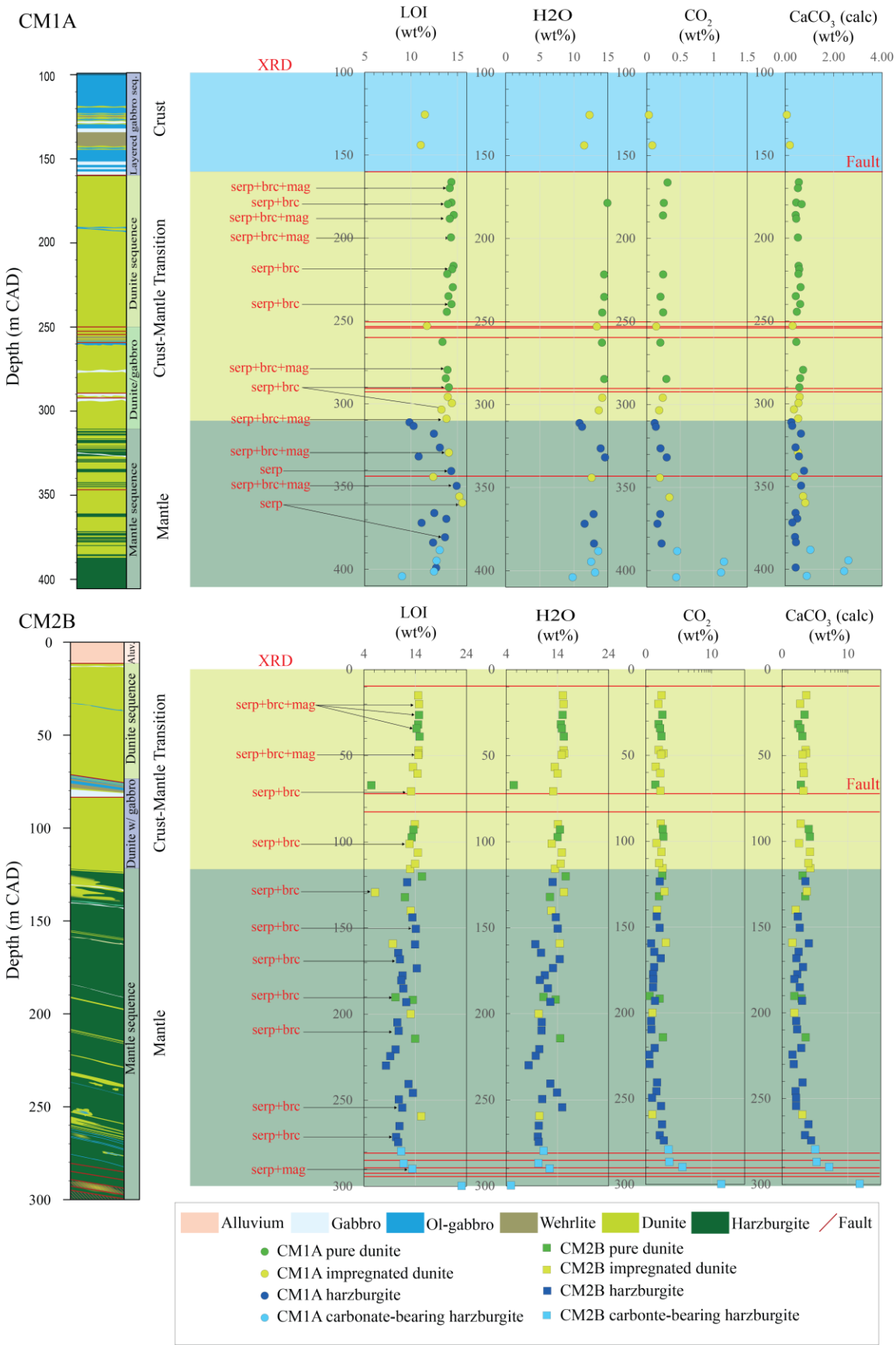
CM1A
LOI (wt%)
H2O (wt%)
CO2 (wt%)
CaCO3 (calc) (wt%)
XRD
Depth (m CAD)
Layered gabbro seq.
Dunite sequence
Dunite/gabbro
Mantle sequence
Crust
Crust-Mantle Transition
Mantle
Fault
serp+brc+mag
serp+brc
serp
CM2B
Alluv.
Dunite sequence
Dunite w/ gabbro
Mantle sequence
Alluvium
Gabbro
Ol-gabbro
Wehrlite
Dunite
Harzburgite
Fault
CM1A pure dunite
CM1A impregnated dunite
CM1A harzburgite
CM1A carbonate-bearing harzburgite
CM2B pure dunite
CM2B impregnated dunite
CM2B harzburgite
CM2B carbonte-bearing harzburgite

Figure 3 Downhole plots of (from left to right) the lithology, LOI (wt.%), H_2O (wt.%), CO_2 (wt.%) and calculated $CaCO_3$ (wt.%) contents in pure dunites, impregnated dunites, harzburgites and carbonate-bearing harzburgites recovered samples at Holes CM1A and CM2B. The thick solid red lines indicate the faults. XRD: X-Ray Diffraction, serp: serpentine, brc: brucite, mag: magnetite.

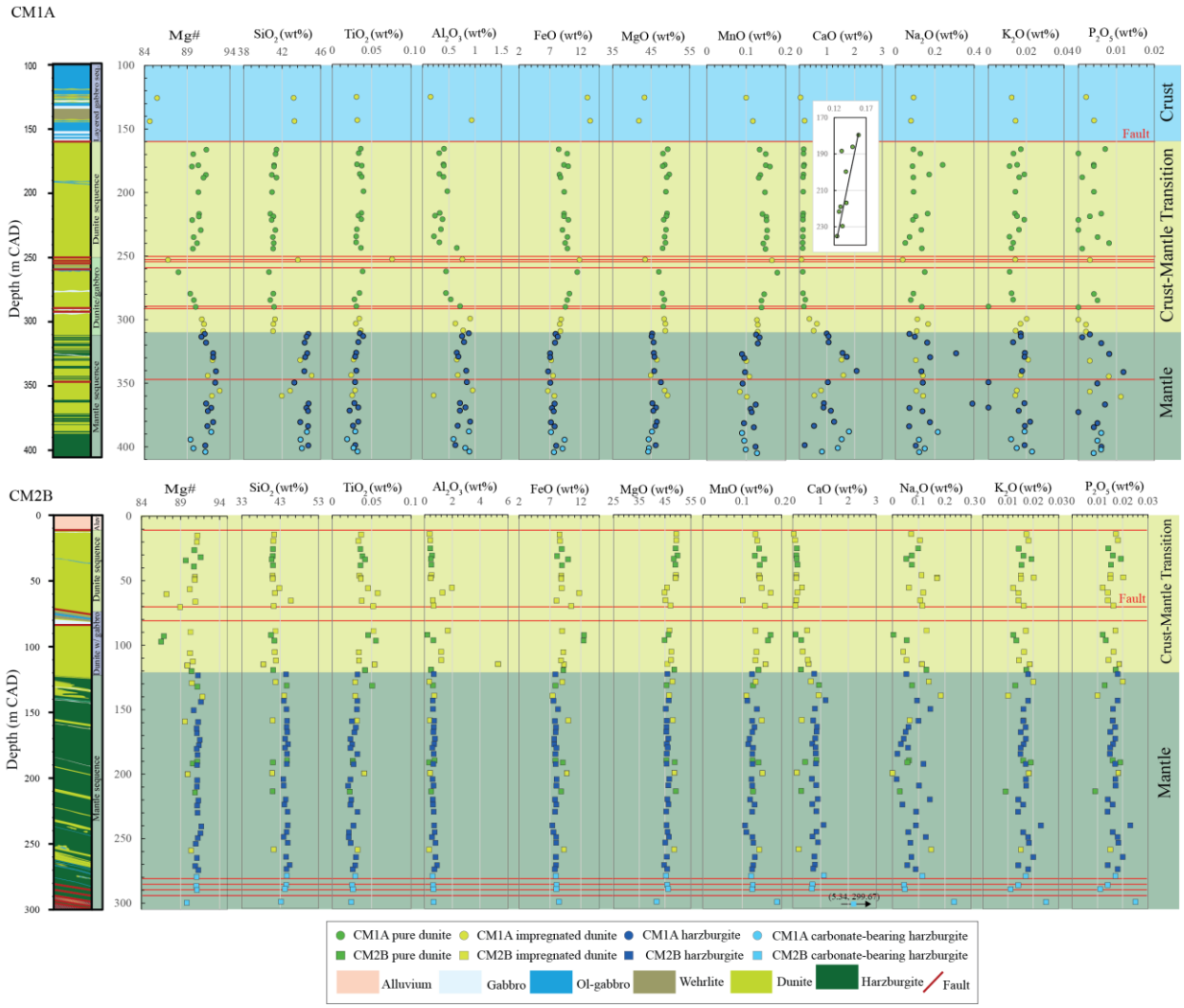

Figure 4 Downhole plots of (from left to right) the lithology, Mg# (cationic 100 x $Mg/(Mg+Fe_{total})$; calculated assuming all Fe as FeO) (mol%), SiO_2 (wt.%), TiO_2 (wt.%), Al_2O_3 (wt.%), FeO (wt.%), MgO (wt.%), MnO (wt.%), CaO (wt.%), Na_2O (wt.%), K_2O (wt.%), and P_2O_5 (wt.%) in whole rock samples recovered at Holes CM1A and CM2B. The thick solid red lines indicate the faults.

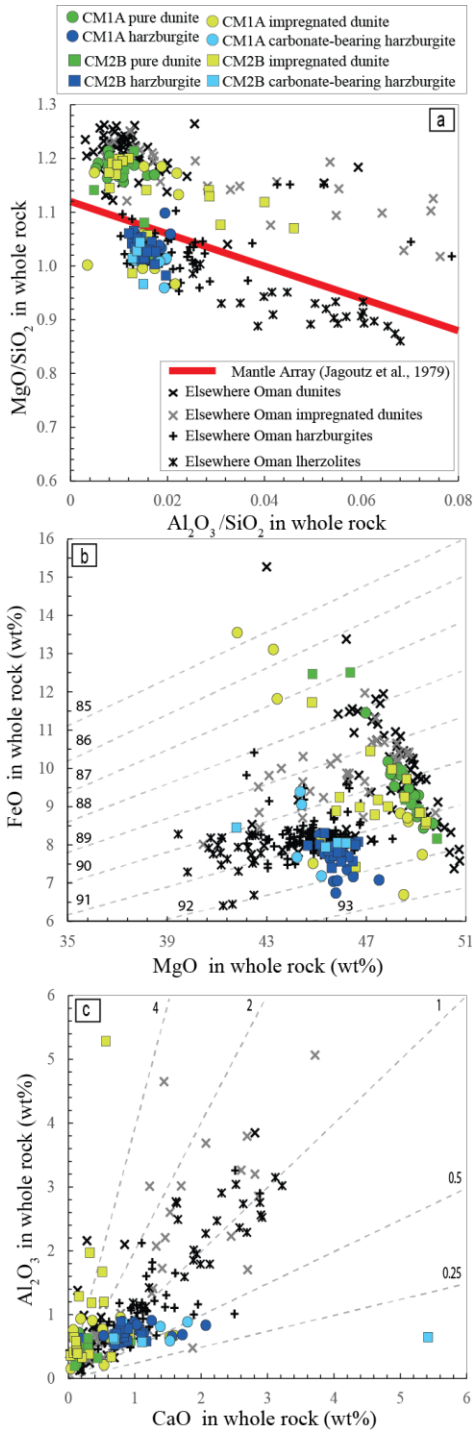

Figure 5 Whole rock major compositions of samples recovered at Holes CM1A and CM2B compared to other crust-mantle transition dunites and mantle harzburgites/lherzolites from the Oman ophiolite (Gerbert-Gaillard, 2002; Godard et al., 2000; Hanghøj et al., 2010; Khedr et al., 2014; Monnier et al., 2006; Nicolle et al., 2016; Rospabé et al., 2018a, 2019a; Takazawa et al., 2003). (a) MgO/SiO_2 versus Al_2O_3/SiO_2, (b) total iron as FeO versus MgO, and (c) Al_2O_3 versus CaO. Compositions are recalculated on a volatile-free basis. Red bar in panel (a) represents the

silicate Earth differentiation trend (or ‘‘terrestrial array”) (Jagoutz et al., 1979). Dashed grey lines in panels (b) and (c) represent constant Mg# and Al_2O_3/CaO ratios respectively.

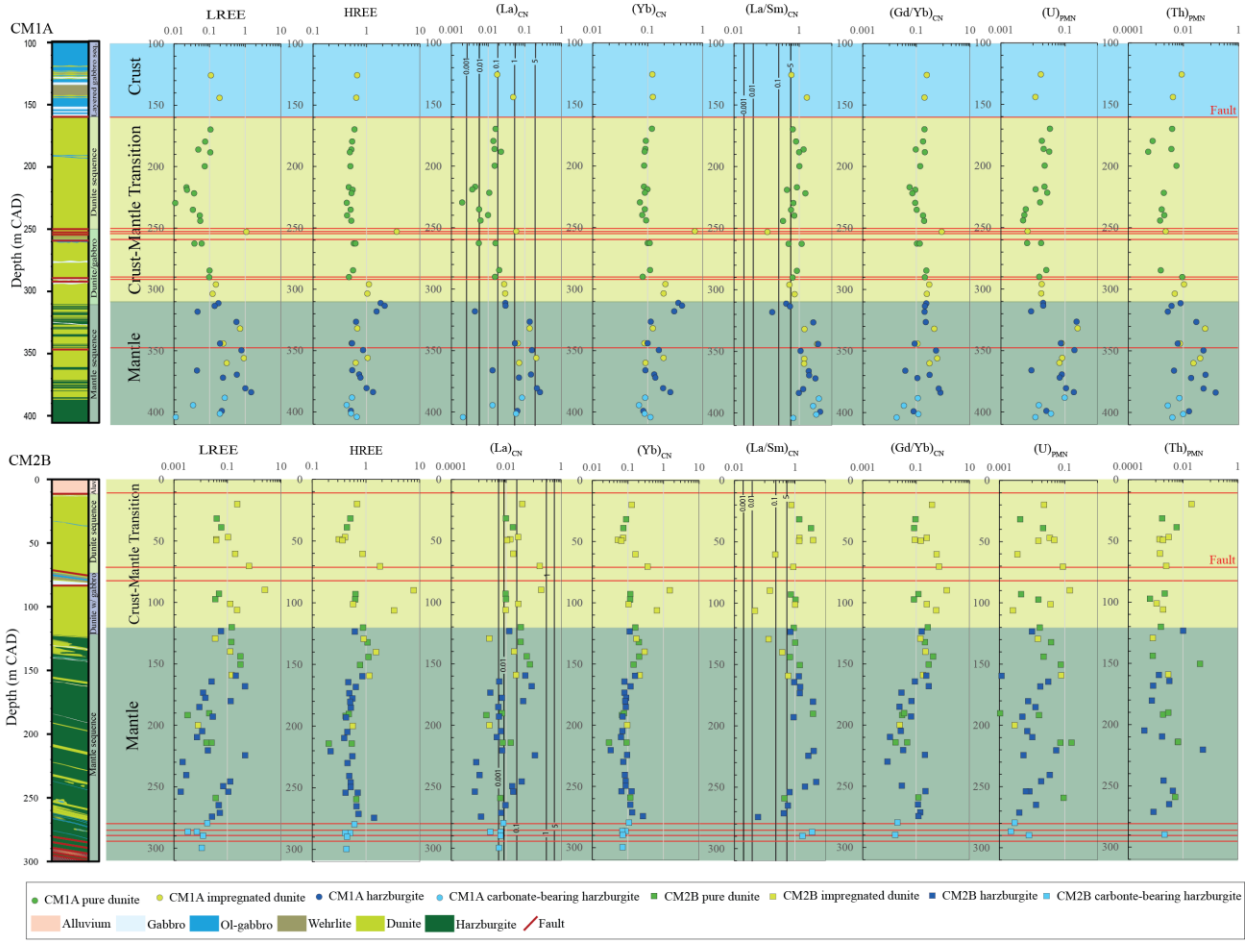

Figure 6 Downhole plots of (from left to right) (LREE: $(La+Ce+Pr+Nd)_{CN}$), (HREE: $(Ho+Er+Tm+Yb+Lu)_{CN}$), $(La)_{CN}$, $(Yb)_{CN}$, $(La/Sm)_{CN}$, $(Gd/Yb)_{CN}$, $(U)_{PMN}$ and $(Th)_{PMN}$ in whole rock samples recovered at Hole CM1A and CM2B (CN: chondrite-normalized; PMN: primitive mantle-normalized). The thick solid red lines indicate the faults, and the thicker solid black lines indicate the $(La)_{CN}$ and $(La/Sm)_{CN}$ concentrations in the most residual peridotites from ‘Plate model’ of Vernières et al. (1997) applied by Godard et al. (2000) (experiment b and d, see Fig.9), the numbers on the black lines indicate the proportions of trapped melt (in percentage) issued from the models. Normalizing chondrite and Primitive Mantle values are from Barrat et al. (2012) and Sun and McDonough (1989) respectively.

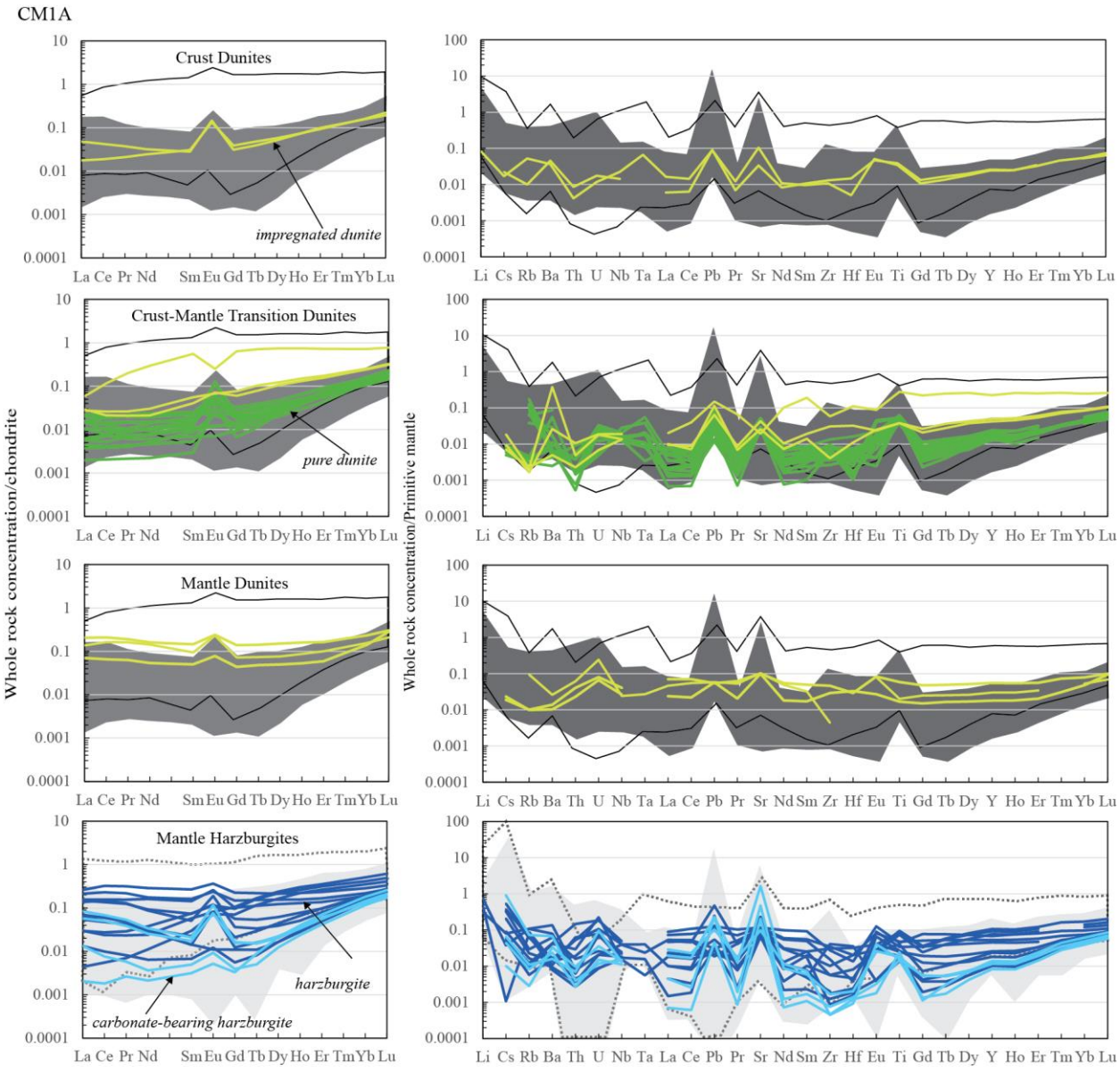

Figure 7a Chondrite-normalized REE and Primitive Mantle-normalized multi-element patterns of pure dunites, impregnated dunites, harzburgites and carbonate-bearing harzburgites from the crust, crust-mantle transition zone and mantle sections recovered at Hole CM1A. Other pure dunites (dark gray field formed) and impregnated dunites (field formed by black line) from the crust-mantle transition, and harzburgites (light gray field) and lherzolites (field formed by dashed line) patterns from the mantle section of the whole Oman ophiolite are reported for comparison (Gerbert-Gaillard, 2002; Girardeau et al., 2002; Godard et al., 2000; Hanghøj et al., 2010; Khedr et al.,2014; Lippard et al., 1986; Monnier et al., 2006; Nicolle et al., 2016, Rospabé et al., 2018a, 2019a; Takazawa et al., 2003). Normalizing chondrite and Primitive Mantle values are from Barrat et al. (2012) and Sun and McDonough (1989) respectively.

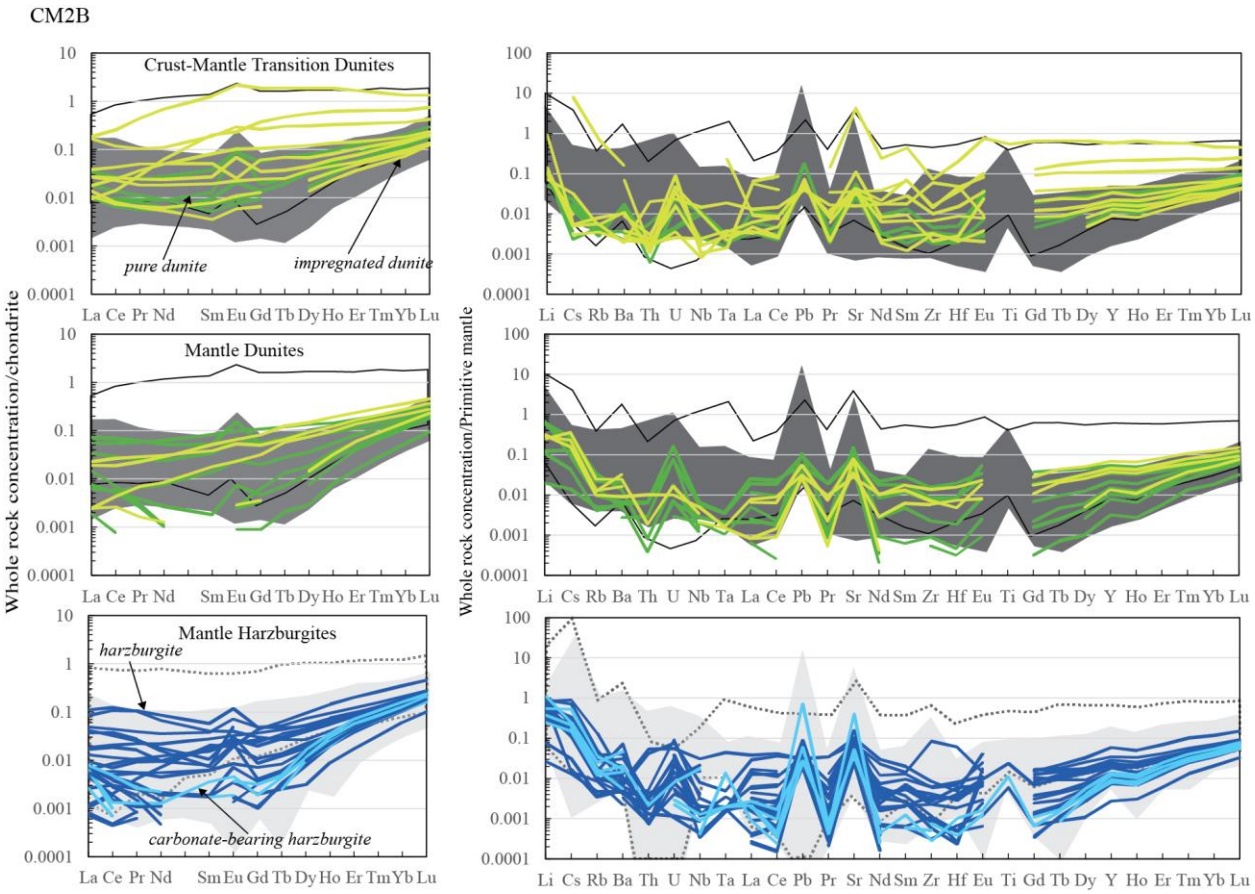

Figure 7b Chondrite-normalized REE and Primitive Mantle-normalized multi-element patterns of pure dunites, impregnated dunites, harzburgites and carbonate-bearing harzburgites from the crust-mantle transition zone and mantle sections recovered at Hole CM2B. Other pure dunites (dark gray field formed) and impregnated dunites (field formed by black line) from the crust-mantle transition, and harzburgites (light gray field) and lherzolites (field formed by dashed line) patterns from the mantle section of the whole Oman ophiolite are reported for comparison (Gerbert-Gaillard, 2002; Girardeau et al., 2002; Godard et al., 2000; Hanghøj et al., 2010; Khedr et al.,2014; Lippard et al., 1986; Monnier et al., 2006; Nicolle et al., 2016, Rospabé et al., 2018a, 2019a; Takazawa et al., 2003). Normalizing chondrite and Primitive Mantle values are from Barrat et al. (2012) and Sun and McDonough (1989) respectively.

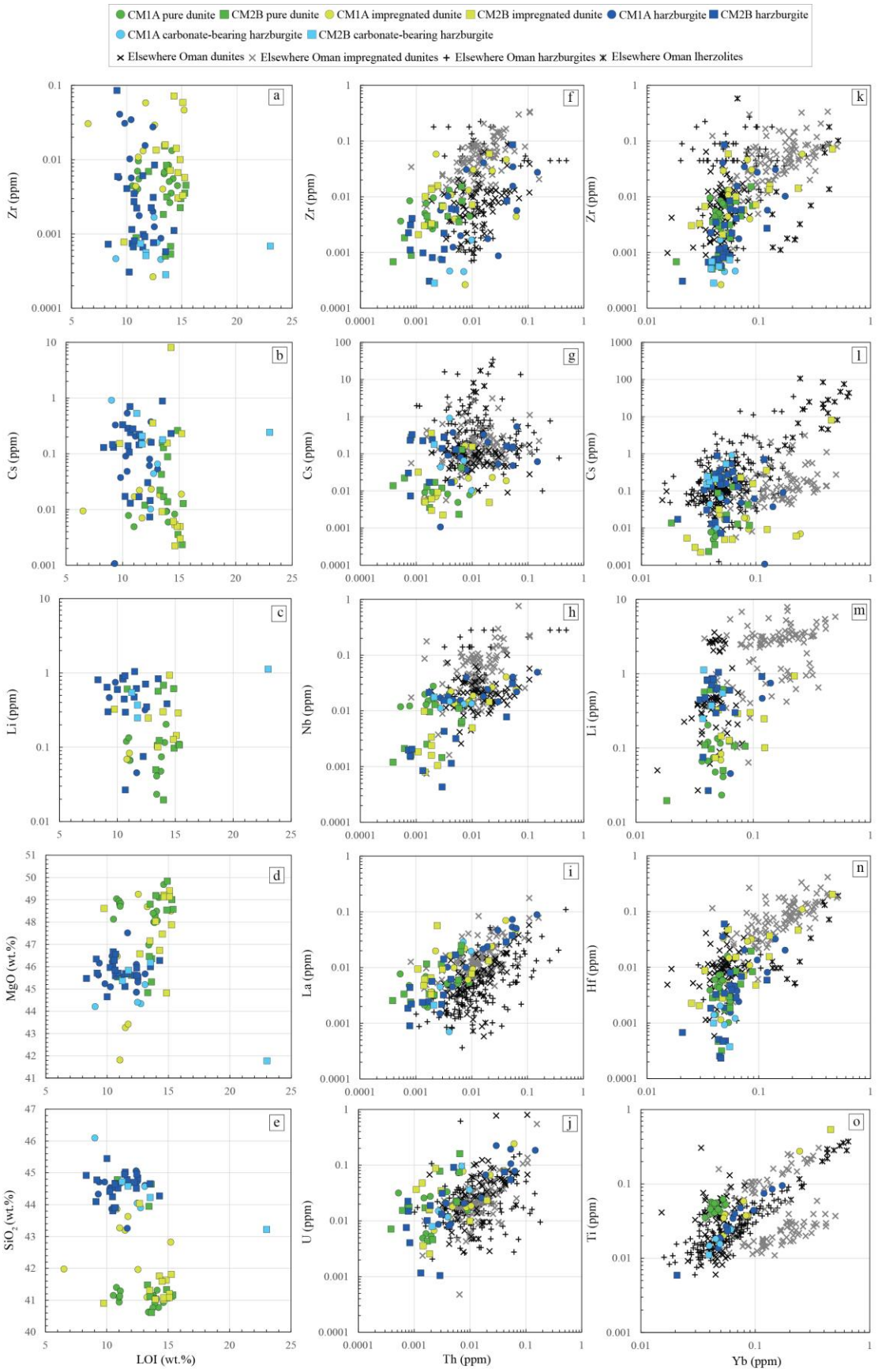
CM1A pure dunite
CM2B pure dunite
CM1A impregnated dunite
CM2B impregnated dunite
CM1A harzburgite
CM2B harzburgite
CM1A carbonate-bearing harzburgite
CM2B carbonate-bearing harzburgite
Elsewhere Oman dunites
Elsewhere Oman impregnated dunites
Elsewhere Oman harzburgites
Elsewhere Oman lherzolites
a
b
c
d
e
f
g
h
i
j
k
l
m
n
o
Zr (ppm)
Cs (ppm)
Li (ppm)
MgO (wt.%)
SiO2 (wt.%)
Nb (ppm)
La (ppm)
U (ppm)
Hf (ppm)
Ti (ppm)
LOI (wt.%)
Th (ppm)
Yb (ppm)

1318

Figure 8 Plots of LOI (wt.%) vs. Zr (ppm), Cs (ppm), Li (ppm), MgO (wt.%), and SiO_2 (wt.%); Th (ppm) vs. Zr (ppm), Cs (ppm), Nb (ppm) , La (ppm), and U (ppm); Yb (ppm) vs. Zr (ppm), Cs (ppm), Li (ppm), Hf (ppm), and Ti (ppm) in dunite and harzburgites recovered at Hole CM1A and CM2B. Other pure dunites, impregnated dunites, harzburgites and lherzolites compositions from the crust-mantle and the mantle section of the whole Oman ophiolite are reported for comparison (Gerbert-Gaillard, 2002; Girardeau et al., 2002; Godard et al., 2000; Hanghøj et al., 2010; Khedr et al., 2014; Lippard et al., 1986; Monnier et al., 2006; Nicolle et al., 2016, Rospabé et al., 2018a, 2019a; Takazawa et al., 2003).

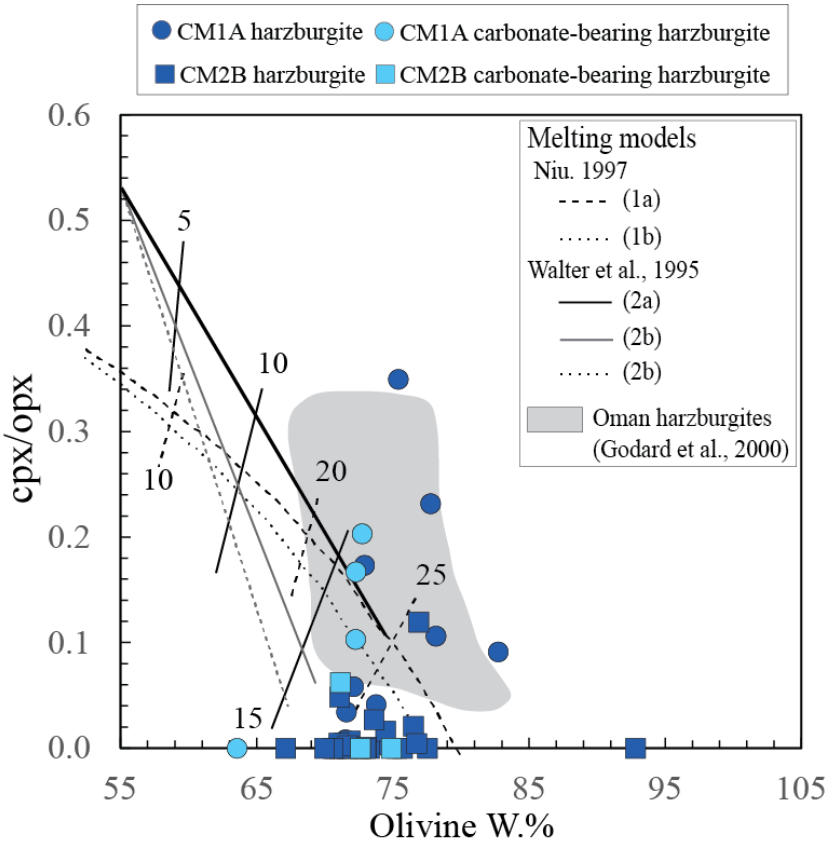

Figure 9 Modal compositions of the analyzed CM harzburgites plotted on a cpx/opx vs. olivine diagram. The field defined by the mantle harzburgites studied in Godard et al., 2000 is reported for comparison. Published melting models are also shown for comparison: model 1 represents the polybaric melting model after Niu (1997), (1a) with and (1b) without excess olivine; model 2 represents the isobaric melting after Walter et al. (1995) at 11 (2a), 16 (2b) and 17 kbar (2c). The initial modal composition is given by Niu (1997) for polybaric melting and was fixed for isobaric melting as: 55% ol, 28% opx, 15% cpx and 2% sp. Numbers refer to percent melting degrees.

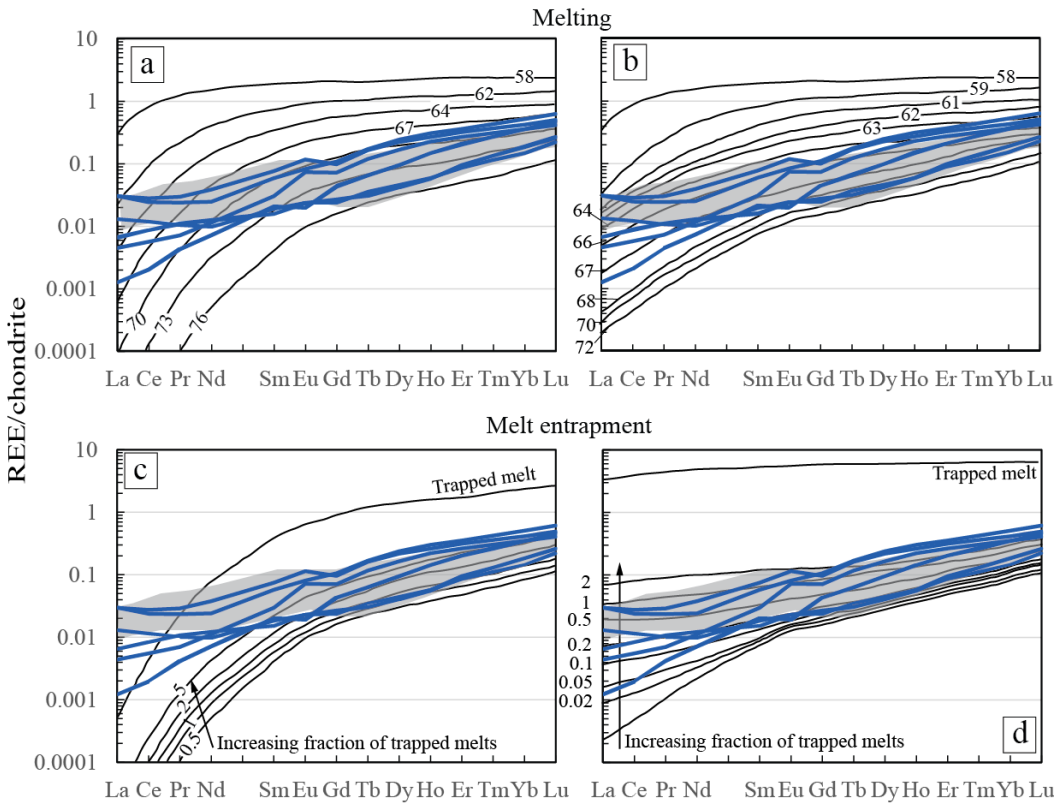

Figure 10 CM1A and CM2B REE linear flat shaped REE patterns (Thicker blue lines) compared to the 'Plate model' of Vernières et al. (1997) applied by Godard et al. (2000) to simulate REE variations in a peridotite affected by partial melting with (a) or without (b) melt infiltration. The chondrite-normalized REE patterns of the Oman harzburgites from Godard et al. (2000) (the gray fields, main harzburgite section) are also shown for comparison. The authors simulate standard incremental melting in model (a) and the percolation of fixed N-MORB melt through molten peridotites in model (b). The peridotite initial modal composition was (spinel free): 57% ol, 28% opx and 15% cpx. The melting reaction was taken from Walter et al. (1995). Mineral/melt partition coefficients are the same as those selected by Bedini & Bodinier (1999). Numbers on the chondrite-normalized REE patterns indicate olivine proportion (in percentage) in residual peridotites. Thicker black lines indicate the REE patterns of the less residual peridotites. In model (a), the most residual peridotite (76% olivine) is produced after 21.1% melt extraction. In model (b), the ratio of infiltrated melt to peridotite varies from 0.02 to 0.19. (Bottom) Modifications of the REE patterns of residual peridotites due to the presence of equilibrium, trapped melt. Models (c) and (d) show the effect of trapped melt on the most residual peridotites of models (a) and (b), respectively (thicker solid lines). Numbers on the REE patterns indicate the proportions of trapped melt (in percentage). Normalizing chondrite values are from Barrat et al. (2012).